Monthly Notices of the ROYAL ASTRONOMICAL SOCIETY

MNRAS 513, 2302–2325 (2022) https://doi.org/10.1093/mnras/stac1063
Advance Access publication 2022 April 27

Atomic data and opacity calculations in La V–X ions for the investigation of kilonova emission spectra

H. Carvajal Gallego,[1] J. C. Berengut,[2] P. Palmeri [1] and P. Quinet [1,3]★

[1] Physique Atomique et Astrophysique, Université de Mons, B-7000 Mons, Belgium
[2] School of Physics, University of New South Wales, Sydney, NSW 2052, Australia
[3] IPNAS, Université de Liège, Sart Tilman, B-4000 Liège, Belgium

Accepted 2022 April 12. Received 2022 April 12; in original form 2022 January 28

ABSTRACT

A new set of radiative parameters for spectral lines in La V–X ions is reported in this paper. These data were determined through the use of a multiplatform approach involving three independent theoretical methods, i.e. the relativistic Hartree–Fock method including core-polarization corrections (HFR + CPOL), the multiconfiguration Dirac–Hartree–Fock (MCDHF) method, and the particle-hole configuration-interaction (PH-CI) method implemented in the AMBiT program. Based on cross-comparisons between the results obtained with these three methods, and from comparisons with the few previously published experimental and theoretical data, the most complete and reliable set of wavelengths, transition probabilities, and oscillator strengths was then used to determine the necessary opacities for the analysis of the spectra emitted in the early phases of kilonovae following neutron star mergers, i.e. for typical conditions corresponding to temperatures $T > 20\,000$ K, a density $\rho = 10^{-10}$ g cm^{-3}, and a time after the merger $t = 0.1$ d.

Key words: atomic data – opacity – neutron star mergers.

1 INTRODUCTION

Lanthanum is the first element of the lanthanide group that extends from $Z = 57$ to 71 in the periodic table. These elements are characterized by rather complex electronic configurations where the 4f orbital is partially filled that leads to a large number of very close energy levels and, consequently, to very high spectral line densities.

It is now well established that such elements are produced in very large quantities during neutron star mergers, such as the one detected on 2017 August 17 (Abbott et al. 2017a,b). Following this coalescence, the spectrum of the kilonova has indeed shown large overabundances of elements heavier than iron (Kasen et al. 2017) among which the lanthanides play a very important role since, due to the extreme richness of their spectra, they strongly contribute to the opacity affecting the light emitted by the kilonova.

In order to determine the light curve of a kilonova, i.e. the evolution of luminosity as a function of time, it is thus necessary to know the atomic structures and the radiative parameters characterizing the lanthanide elements in various degrees of ionization. In recent years, some progress has been made in this direction in that many new spectroscopic parameters related to lowly charged lanthanide ions were computed by Carvajal Gallego, Palmeri & Quinet (2021) for Ce II–IV ($Z = 58$), by Gaigalas et al. (2019) for Nd II–IV ($Z = 60$), by Gaigalas et al. (2020) for Er III ($Z = 68$), by Radžiūtė et al. (2020) for the ions between Pr II ($Z = 59$) and Gd II ($Z = 64$), by Radžiūtė et al. (2021) for the ions between Tb II ($Z = 65$) and Yb II ($Z = 70$), and by Tanaka et al. (2020) for the ions between La I–IV ($Z = 57$) and Lu I–IV ($Z = 71$). In these works, the opacities due to the considered ions were also estimated, allowing to build a synthetic spectrum for the kilonova in the temperature range 0–20 000 K.

In order to analyse the spectra emitted during the early phases of kilonovae, i.e. for temperatures beyond 20 000 K, it is necessary to extend the above-mentioned studies to higher ionization degrees of lanthanide atoms, for which very little (if any) data are available in the literature. A first step in this direction has been realized recently in one of our works focused on Ce V–X ions (Carvajal Gallego et al. 2022). In the latter, the radiative parameters were calculated for millions of spectral lines from which the monochromatic opacities were evaluated for each of these cerium ions. The accuracy of the atomic calculations could be estimated by comparing the results obtained using three independent theoretical methods, namely the relativistic Hartree–Fock method including core-polarization effects (HFR + CPOL), the multiconfiguration Dirac–Hartree–Fock (MCDHF) method, and the particle-hole configuration-interaction (PH-CI) method implemented in the AMBiT code. The same multiplatform approach was implemented in this work to model the atomic systems and calculate the opacities corresponding to La V–X ions, for which we obtained a new reliable and consistent set of transition probabilities and oscillator strengths for the first time.

2 AVAILABLE ATOMIC DATA

Over the last decades, spectral line observations allowing to establish experimental energy levels were published in each of the lanthanum ions between La V and La X. All these studies were performed using a variety of normal incidence and grazing incidence spectrographs while the sources for exciting the spectra were either a conventional triggered spark or a laser-produced plasma.

★ E-mail: pascal.quinet@umons.ac.be

Table 1. Configurations included in the HFR + CPOL calculations for La V–X ions.

La V	La VI	La VII	La VIII	La IX	La X
Odd parity	Even parity	Odd parity	Even parity	Odd parity	Even parity
$5s^25p^5$	$5s^25p^4$	$5s^25p^3$	$5s^25p^2$	$5s^25p$	$5s^2$
$5s^25p^46p$	$5s^25p^36p$	$5s^25p^26p$	$5s^25p6p$	$5s^26p$	5s5d
$5s^25p^47p$	$5s^25p^37p$	$5s^25p^27p$	$5s^25p7p$	$5s^27p$	5s6d
$5s^25p^48p$	$5s^25p^38p$	$5s^25p^28p$	$5s^25p8p$	$5s^28p$	5s7d
$5s^25p^44f$	$5s^25p^34f$	$5s^25p^24f$	$5s^25p4f$	$5s^24f$	5s8d
$5s^25p^45f$	$5s^25p^35f$	$5s^25p^25f$	$5s^25p5f$	$5s^25f$	5s6s
$5s^25p^46f$	$5s^25p^36f$	$5s^25p^26f$	$5s^25p6f$	$5s^26f$	5s7s
$5s^25p^47f$	$5s^25p^37f$	$5s^25p^27f$	$5s^25p7f$	$5s^27f$	5s8s
$5s^25p^48f$	$5s^25p^38f$	$5s^25p^28f$	$5s^25p8f$	$5s^28f$	5s5g
$5s^25p^34f^2$	$5s^25p^24f^2$	$5s^25p4f^2$	$5s^24f^2$	5s5p5d	5s6g
$5s^25p^35d^2$	$5s^25p^25d^2$	$5s^25p5d^2$	$5s^25d^2$	5s5p6d	5s7g
$5s^25p^36s^2$	$5s^25p^26s^2$	$5s^25p6s^2$	$5s^26s^2$	5s5p7d	5s8g
$5s^25p^35d6s$	$5s^25p^25d6s$	$5s^25p5d6s$	$5s^25d6s$	5s5p8d	$5p^2$
$5s5p^55d$	$5s5p^45d$	$5s5p^35d$	$5s5p^25d$	5s5p6s	$5d^2$
$5s5p^56d$	$5s5p^46d$	$5s5p^36d$	$5s5p^26d$	5s5p7s	$4f^2$
$5s5p^57d$	$5s5p^47d$	$5s5p^37d$	$5s5p^27d$	5s5p8s	5p6p
$5s5p^58d$	$5s5p^48d$	$5s5p^38d$	$5s5p^28d$	5s4f5d	5p7p
$5s5p^56s$	$5s5p^46s$	$5s5p^36s$	$5s5p^26s$	5s4f6d	5p8p
$5s5p^57s$	$5s5p^47s$	$5s5p^37s$	$5s5p^27s$	5s4f7d	5p4f
$5s5p^58s$	$5s5p^48s$	$5s5p^38s$	$5s5p^28s$	5s4f8d	5p6f
$5s5p^44f5d$	$5s5p^34f5d$	$5s5p^24f5d$	5s5p4f5d	5s4f6s	5p7f
$5s5p^44f6d$	$5s5p^34f6d$	$5s5p^24f6d$	5s5p4f6d	5s4f7s	5p8f
$5s5p^44f7d$	$5s5p^34f7d$	$5s5p^24f7d$	5s5p4f7d	5s4f8s	4f6p
$5s5p^44f8d$	$5s5p^34f8d$	$5s5p^24f8d$	5s5p4f8d	$5p^3$	4f7p
$5s5p^44f6s$	$5s5p^34f6s$	$5s5p^24f6s$	5s5p4f6s	$4f^3$	4f8p
$5s5p^44f7s$	$5s5p^34f7s$	$5s5p^24f7s$	5s5p4f7s	$5p4f^2$	
$5s5p^44f8s$	$5s5p^34f8s$	$5s5p^24f8s$	5s5p4f8s	$5p^24f$	
$5p^44f^3$	$5p^6$	$5p^5$	$5p^4$		
$5p^54f^2$	$5p^44f^2$	$5p^24f^3$	$5p4f^3$		
$5p^64f$	$5p^54f$	$5p^34f^2$	$5p^24f^2$		
		$5p^44f$	$5p^34f$		
Even parity	Odd parity	Even parity	Odd parity	Even parity	Odd parity
$5s^25p^46s$	$5s^25p^36s$	$5s^25p^26s$	$5s^25p6s$	$5s^26s$	5s5p
$5s^25p^47s$	$5s^25p^37s$	$5s^25p^27s$	$5s^25p7s$	$5s^27s$	5s6p
$5s^25p^48s$	$5s^25p^38s$	$5s^25p^38s$	$5s^25p8s$	$5s^28s$	5s7p
$5s^25p^45d$	$5s^25p^35d$	$5s^25p^25d$	$5s^25p5d$	$5s^25d$	5s8p
$5s^25p^46d$	$5s^25p^36d$	$5s^25p^26d$	$5s^25p6d$	$5s^26d$	5s4f
$5s^25p^47d$	$5s^25p^37d$	$5s^25p^27d$	$5s^25p7d$	$5s^27d$	5s5f
$5s^25p^48d$	$5s^25p^38d$	$5s^25p^28d$	$5s^25p8d$	$5s^28d$	5s6f
$5s^25p^45g$	$5s^25p^35g$	$5s^25p^25g$	$5s^25p5g$	$5s^25g$	5s7f
$5s^25p^46g$	$5s^25p^36g$	$5s^25p^26g$	$5s^25p6g$	$5s^26g$	5s8f
$5s^25p^47g$	$5s^25p^37g$	$5s^25p^27g$	$5s^25p7g$	$5s^27g$	5p5d
$5s^25p^48g$	$5s^25p^38g$	$5s^25p^28g$	$5s^25p8g$	$5s^28g$	5p6d
$5s^25p^34f5d$	$5s^25p^24f5d$	$5s^25p4f5d$	$5s^24f5d$	$5s5p^2$	5p7d
$5s^25p^34f6s$	$5s^25p^24f6s$	$5s^25p4f6s$	$5s^24f6s$	5s5p6p	5p8d
$5s5p^6$	$5s5p^5$	$5s5p^4$	$5s5p^3$	5s5p7p	5p6s
$5s5p^56p$	$5s5p^46p$	$5s5p^36p$	$5s5p^26p$	5s5p8p	5p7s
$5s5p^57p$	$5s5p^47p$	$5s5p^37p$	$5s5p^27p$	5s5p4f	5p8s
$5s5p^58p$	$5s5p^48p$	$5s5p^38p$	$5s5p^28p$	5s5p5f	4f5d
$5s5p^54f$	$5s5p^44f$	$5s5p^34f$	$5s5p^24f$	5s5p6f	4f6d
$5s5p^55f$	$5s5p^45f$	$5s5p^35f$	$5s5p^25f$	5s5p7f	4f7d
$5s5p^56f$	$5s5p^46f$	$5s5p^36f$	$5s5p^26f$	5s5p8f	4f8d
$5s5p^57f$	$5s5p^47f$	$5s5p^37f$	$5s5p^27f$	$5s4f^2$	4f6s
$5s5p^58f$	$5s5p^48f$	$5s5p^38f$	$5s5p^28f$	5s4f6p	4f7s
$5s5p^44f^2$	$5s5p^34f^2$	$5s5p^24f^2$	$5s5p4f^2$	5s4f7p	4f8s
$5s5p^44f6p$	$5s5p^34f6p$	$5s5p^24f6p$	5s5p4f6p	5s4f8p	
$5s5p^44f7p$	$5s5p^34f7p$	$5s5p^24f7p$	5s5p4f7p	$5p^25d$	
$5s5p^44f8p$	$5s5p^34f8p$	$5s5p^24f8p$	5s5p4f8p	$4f^25d$	
$5p^65d$	$5p^55d$	$5p^45d$	$5p^35d$	5p4f5d	
$5p^44f^25d$	$5p^44f5d$	$5p^24f^25d$	$5p4f^25d$		
$5p^54f5d$		$5p^34f5d$	$5p^24f5d$		

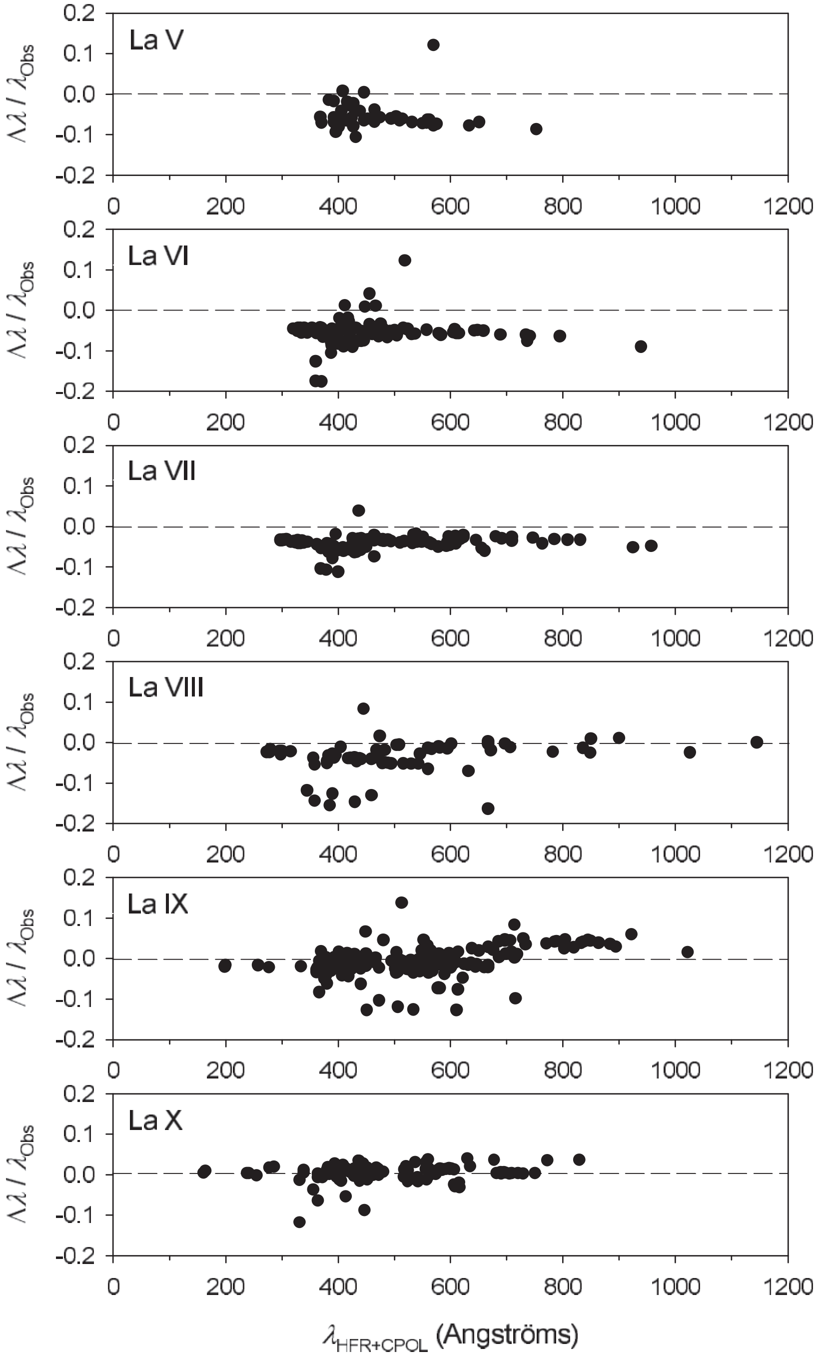

Figure 1. Deviation between HFR + CPOL and observed wavelengths, $\Delta\lambda/\lambda_{Obs}$ (with $\Delta\lambda = \lambda_{HFR+CPOL} - \lambda_{Obs}$) as a function of $\lambda_{HFR+CPOL}$ for spectral lines in La V–X ions. Experimental wavelengths are from Epstein & Reader (1976) for La V, from Gayasov et al. (1997) for La VI, from Gayasov et al. (1998) for La VII, from Tauheed et al. (2008) for La VIII, from Gayasov & Joshi (1998) and Churilov & Joshi (2001) for La IX, and from Ryabtsev et al. (2002) for La X.K

More precisely, in La V, 47 lines were recorded by Epstein & Reader (1976) in the 389–825 Å wavelength region leading to the identification of 29 levels belonging to the $5s^25p^5$, $5s^25p^45d$, $5s^25p^46s$, and $5s5p^6$ configurations. 103 lines appearing between 335 and 1031 Å were classified by Gayasov, Joshi & Tauheed (1997) as La VI transitions from the $5s^25p^4$ ground configuration to $5s^25p^35d$, $5s^25p^36s$, and $5s5p^5$ configurations, giving rise to the establishment of five even-parity and 42 odd-parity levels. In La VII, Gayasov, Joshi & Tauheed (1998) observed, in the 307–1005 Å wavelength range, 102 lines identified as being due to transitions from the five levels of the $5s^25p^3$ configuration to 37 levels (among the 44 possible levels) of the $5s^25p^25d$, $5s^25p^26s$, and $5s5p^4$ even configurations. In La VIII, all the five levels of the $5s^25p^2$ ground configuration and all the 26 levels belonging to the $5s^25p5d$, $5s^25p6s$, and $5s5p^3$ odd configurations were established by Tauheed, Joshi & Marshall (2008) thanks to the measurement of 71 lines between 280 and 1145 Å. In 2001, the analysis of complex ($5p^3$ + $5s5p5d + 4f5p^2 + 5s^26p + 5s^25f$)–($5s5p^2$, $5s4f5p + 5s^25d$) transition arrays in La IX was carried out by Churilov & Joshi (2001) who classified 155 lines in the 363–870 Å region. This study completed the previous investigation of the La IX spectrum by Gayasov & Joshi (1998) who identified 49 lines belonging to the ($5s^25p$ + $5s^24f$)–

Table 2. Computational strategies used in MCDHF calculations for La V–X ions.

Calculation	La V	La VI	La VII	La VIII	La IX	La X
MR	Odd parity	Even parity	Odd parity	Even parity	Odd parity	Even parity
	$5s^25p^5$	$5s^25p^4$	$5s^25p^3$	$5s^25p^2$	$5s^25p$	$5s^2$
	$5s^25p^44f$	$5s^25p^34f$	$5s^25p^24f$	$5s^25p4f$	$5s^24f$	$5p^2$
	$5s^25p^34f^2$	$5s^25p^24f^2$	$5s^25p4f^2$	$5s^24f^2$	5s5p5d	5p4f
					$5p^24f$	5s5d
					$5p4f^2$	
					$5p^3$	
	Even parity	Odd parity	Even parity	Odd parity	Even parity	Odd parity
	$5s5p^6$	$5s5p^5$	$5s5p^4$	$5s5p^3$	$5s5p^2$	5s5p
	$5s5p^54f$	$5s5p^44f$	$5s5p^34f$	$5s5p^24f$	5s5p4f	5s4f
	$5s^25p^45d$	$5s^25p^35d$	$5s^25p^25d$	$5s^25p5d$	$5s^25d$	4f5d
					$5s4f^2$	5p5d
VV1	{5s,5p,5d,5f,5g}	{5s,5p,5d,5f,5g}	{5s,5p,5d,5f,5g}	{5s,5p,5d,5f,5g}	{5s,5p,5d,5f,5g}	{5s,5p,5d,5f,5g}
VV2	{6s,6p,6d,6f,5g}	{6s,6p,6d,6f,5g}	{6s,6p,6d,6f,5g}	{6s,6p,6d,6f,5g}	{6s,6p,6d,6f,5g}	{6s,6p,6d,6f,5g}
VV3	{7s,7p,7d,6f,5g}	{7s,7p,7d,6f,5g}	{7s,7p,7d,6f,5g}	{7s,7p,7d,6f,5g}	{7s,7p,7d,6f,5g}	{7s,7p,7d,6f,5g}
CV	{5s,5p,5d,5f,5g}	{5s,5p,5d,5f,5g}	{5s,5p,5d,5f,5g}	{5s,5p,5d,5f,5g}	{5s,5p,5d,5f,5g}	{5s,5p,5d,5f,5g}
CSFs	4389 357	3707 264	2084 541	839 430	1222 461	271 640

($5s^25d + 5s^26s + 5s^25g + 5s5p^2 + 5s5p4f$) transition arrays. Both together, these latter works allowed the classification of 64 odd levels and 35 even levels in La IX. Finally, the spectrum of La X was analysed by Ryabtsev, Churilov & Joshi (2002) who listed 140 lines between 117 and 801 Å as being due to transitions from the $5s^2$, $5p^2$, 4f5p, 5s5d, and 5s6s even configurations to the 5s5p, 5s6p, 5s5f, 5p5d, 4f5s, and 4f5d odd configurations. This work allowed the classification of 24 and 40 energy levels in even and odd parities, respectively, confirming (except for one level) and extending the earlier study of Gayasov, Joshi & Ryabtsev (1999).

Regarding the radiative decay rates for electric dipole transitions in La V–X ions, very few results have been published so far since only a few results are available for La IX and La X. In both cases, transition probabilities were computed for experimentally observed lines using the pseudo-relativistic Hartree–Fock (HFR) method of Cowan (1981). To be more precise, it should be noted that the La IX calculations were undertaken by Churilov & Joshi (2001) by means of a HFR model including the $5s^25p$, $5s^24f$, $5s^26p$, $5s^25f$, $5p^3$, 5s5p5d, $4f5p^2$, $4f^25p$, $4f^3$, 5s4f5d, and 5s5p6s odd configurations and the $5s5p^2$, $5s^25d$, $5s^26s$, $5s^26d$, $5s^25g$, 5s5p4f, $5s4f^2$, and 5s5p6p even configurations while the La X *gA* values were obtained by Ryabtsev et al. (2002) with a HFR model including the $5s^2$, $5p^2$, $4f^2$, 4f5d, 5s*nd* ($n = 5, 6$), 5s5g, 5s*ns* ($n = 6, 7$), $4d^94f^25s$, $4d^95s^26s$, and $4d^95s^25d$ even configurations and the 5s*np* ($n = 5, 6$), 5s*nf* ($n = 4, 5$), 5p6s, $4d^95s^25p$, $4d^95s^24f$, and $4d^94f^25p$ odd configurations. Let us also mention that the radiative parameters of $5s^2$–5s5p transitions were theoretically investigated along the cadmium isoelectronic sequence, including La X, by Chou & Huang (1992), Curtis et al. (2000), Biémont et al. (2000), and Reshetnikov et al. (2008).

3 ATOMIC STRUCTURE CALCULATIONS

3.1 HFR + CPOL method

In a first step, we used the pseudo-relativistic Hartree–Fock method including core-polarization effects (HFR + CPOL) for calculating the atomic structures and radiative parameters in La V–X ions. This method, originally introduced by Cowan (1981) and modified to account for core–valence correlation effects via a core-polarization potential and a correction to the electric dipole operator, as described by Quinet et al. (1999, 2002), and recalled by Carvajal Gallego et al. (2022), has proven its ability to provide reliable atomic data in many heavy ions, especially when an important number of radiative transitions must be considered for astrophysical and laboratory plasma studies (see e.g. Quinet 2017; Quinet & Palmeri 2020).

In this work, for each lanthanum ion considered, we adopted a physical model in which valence–valence correlations were assumed to take place outside a Pd-like La XII ionic core. For this purpose, the interacting configurations listed in Table 1 were introduced explicitly in the calculations while the core-polarization parameters corresponding to the dipole polarizability of the core and the cut-off radius were chosen as $\alpha_d = 0.47\ a_0^3$ and $r_c = 0.76\ a_0$, respectively. The former value was taken from Fraga, Karwowski & Saxena (1976) while the latter one was obtained by taking the average value $\langle r \rangle$ for the outermost 4d core orbital, as calculated using the HFR method.

The accuracy of the HFR + CPOL atomic structure calculations was first assessed through comparisons with available experimental data. More precisely, a good overall agreement (smaller than 5 per cent in most cases) was found when comparing the computed wavelengths with those measured in laboratory by Epstein & Reader (1976) for La V, by Gayasov et al. (1997) for La VI, by Gayasov et al. (1998) for La VII, by Tauheed et al. (2008) for La VIII, by Gayasov & Joshi (1998) and Churilov & Joshi (2001) for La IX, and by Ryabtsev et al. (2002) for La X for which the average differences $\Delta\lambda/\lambda_{\rm Obs}$ (with $\Delta\lambda = \lambda_{\rm HFR+CPOL} - \lambda_{\rm Obs}$) were found to be equal to -0.055 ± 0.035 (La V), -0.054 ± 0.032 (La VI), -0.042 ± 0.018 (La VII), -0.037 ± 0.041 (La VIII), -0.010 ± 0.033 (La IX), and 0.005 ± 0.020 (La X). The full comparison between HFR + CPOL and available experimental wavelengths is shown in Fig. 1 for all the lanthanum ions considered in this work.

3.2 MCDHF method

In a second step, the fully relativistic multiconfiguration Dirac–Hartree–Fock (MCDHF) method described by Grant (2007) and Froese Fischer et al. (2016) was used with the latest version of General Relativistic Atomic Structure Package (GRASP), i.e. GRASP2018 (Froese Fischer et al. 2019), for computing the atomic structures and radiative processes in La V–X ions. For each of these ions, a multireference (MR) of spectroscopic configurations, among which all transitions were calculated, was chosen and, from this MR, the valence–valence (VV) and core–valence (CV) interactions

Table 3. Transition probabilities (gA) and oscillator strengths ($\log gf$) for experimentally observed lines in La V.

λ_{obs} (Å)^a	Transition^a		gA (s^{-1})^b	$\log gf$ ^{b}
	Lower level	Upper level		
389.034	$5s^25p^5\ ^2P^o_{3/2}$	$5s^25p^46s(^1D_2,1/2)_{3/2}$	3.25E + 10	− 0.14
390.722	$5s^25p^5\ ^2P^o_{3/2}$	$5s^25p^46s(^1D_2,1/2)_{5/2}$	4.38E + 10	− 0.05
398.531	$5s^25p^5\ ^2P^o_{3/2}$	$5s^25p^4(^3P)5d\ ^2D_{3/2}$	1.94E + 09	− 1.40
399.343	$5s^25p^5\ ^2P^o_{3/2}$	$5s^25p^46s(^3P_1,1/2)_{1/2}$	1.23E + 09	− 1.55
405.097	$5s^25p^5\ ^2P^o_{3/2}$	$5s^25p^46s(^3P_1,1/2)_{3/2}$	3.95E + 10	− 0.01
416.132	$5s^25p^5\ ^2P^o_{3/2}$	$5s^25p^46s(^3P_0,1/2)_{1/2}$	1.23E + 09	− 1.55
421.547	$5s^25p^5\ ^2P^o_{3/2}$	$5s^25p^4(^3P)5d\ ^2P_{1/2}$	1.23E + 09	− 1.55
423.074	$5s^25p^5\ ^2P^o_{3/2}$	$5s^25p^4(^1S)5d\ ^2D_{5/2}$	3.03E + 10	− 0.13
424.784	$5s^25p^5\ ^2P^o_{1/2}$	$5s^25p^46s(^1D_2,1/2)_{3/2}$	2.71E + 08	− 2.15
432.108	$5s^25p^5\ ^2P^o_{3/2}$	$5s^25p^4(^3P)5d\ ^2P_{3/2}$	2.38E + 11	0.76
435.275	$5s^25p^5\ ^2P^o_{3/2}$	$5s^25p^4(^3P)5d\ ^2D_{5/2}$	4.42E + 11	1.02
436.135	$5s^25p^5\ ^2P^o_{1/2}$	$5s^25p^4(^3P)5d\ ^2D_{3/2}$	3.07E + 11	0.87
436.843	$5s^25p^5\ ^2P^o_{3/2}$	$5s^25p^4(^1D)5d\ ^2S_{1/2}$	1.39E + 11	0.51
437.107	$5s^25p^5\ ^2P^o_{1/2}$	$5s^25p^46s(^3P_1,1/2)_{1/2}$	1.16E + 10	− 0.50
437.551	$5s^25p^5\ ^2P^o_{3/2}$	$5s^25p^46s(^3P_2,1/2)_{3/2}$	2.00E + 10	− 0.27
444.010	$5s^25p^5\ ^2P^o_{1/2}$	$5s^25p^46s(^3P_1,1/2)_{3/2}$	5.57E + 08	− 1.78
444.067	$5s^25p^5\ ^2P^o_{3/2}$	$5s^25p^46s(^3P_2,1/2)_{5/2}$	6.87E + 09	− 0.75
450.405	$5s^25p^5\ ^2P^o_{3/2}$	$5s^25p^4(^1S)5d\ ^2D_{3/2}$	2.00E + 10	− 0.27
457.303	$5s^25p^5\ ^2P^o_{1/2}$	$5s^25p^46s(^3P_0,1/2)_{1/2}$	6.73E + 08	− 1.71
463.848	$5s^25p^5\ ^2P^o_{1/2}$	$5s^25p^4(^3P)5d\ ^2P_{1/2}$	1.16E + 10	− 0.50
476.667	$5s^25p^5\ ^2P^o_{1/2}$	$5s^25p^4(^3P)5d\ ^2P_{3/2}$	5.57E + 08	− 1.71
482.164	$5s^25p^5\ ^2P^o_{3/2}$	$5s^25p^4(^1D)5d\ ^2F_{5/2}$	3.74E + 09	− 0.94
482.434	$5s^25p^5\ ^2P^o_{1/2}$	$5s^25p^4(^1D)5d\ ^2S_{1/2}$	6.75E + 09	− 0.72
483.298	$5s^25p^5\ ^2P^o_{1/2}$	$5s^25p^46s(^3P_2,1/2)_{3/2}$	1.02E + 10	− 0.48
498.081	$5s^25p^5\ ^2P^o_{3/2}$	$5s^25p^4(^3P)5d\ ^2F_{5/2}$	1.85E + 09	− 1.22
499.028	$5s^25p^5\ ^2P^o_{1/2}$	$5s^25p^4(^1S)5d\ ^2D_{3/2}$	1.02E + 10	− 0.48
503.583	$5s^25p^5\ ^2P^o_{3/2}$	$5s^25p^4(^1D)5d\ ^2D_{5/2}$	1.42E + 09	− 1.32
508.147	$5s^25p^5\ ^2P^o_{3/2}$	$5s^25p^4(^1D)5d\ ^2P_{3/2}$	1.05E + 07	− 3.30
525.712	$5s^25p^5\ ^2P^o_{3/2}$	$5s^25p^4(^1D)5d\ ^2D_{3/2}$	5.50E + 08	− 1.70
526.755	$5s^25p^5\ ^2P^o_{3/2}$	$5s^25p^4(^3P)5d\ ^4P_{5/2}$	1.79E + 09	− 1.18
531.069	$5s^25p^5\ ^2P^o_{3/2}$	$5s^25p^4(^3P)5d\ ^4F_{3/2}$	3.44E + 09	− 0.89
533.233	$5s^25p^5\ ^2P^o_{3/2}$	$5s^25p^4(^3P)5d\ ^4F_{5/2}$	3.37E + 09	− 0.89
540.203	$5s^25p^5\ ^2P^o_{3/2}$	$5s^25p^4(^1D)5d\ ^2P_{1/2}$	1.68E + 09	− 1.19
544.805	$5s^25p^5\ ^2P^o_{3/2}$	$5s^25p^4(^3P)5d\ ^4P_{1/2}$	4.14E + 08	− 1.79
547.437	$5s^25p^5\ ^2P^o_{3/2}$	$5s^25p^4(^3P)5d\ ^4P_{3/2}$	8.48E + 08	− 1.47
570.903	$5s^25p^5\ ^2P^o_{1/2}$	$5s^25p^4(^1D)5d\ ^2P_{3/2}$	1.06E + 08	− 2.35
593.181	$5s^25p^5\ ^2P^o_{1/2}$	$5s^25p^4(^1D)5d\ ^2D_{3/2}$	2.87E + 08	− 1.88
597.698	$5s^25p^5\ ^2P^o_{3/2}$	$5s^25p^4(^3P)5d\ ^4D_{3/2}$	3.75E + 07	− 2.75
600.009	$5s^25p^5\ ^2P^o_{1/2}$	$5s^25p^4(^3P)5d\ ^4F_{3/2}$	1.67E + 08	− 2.11
600.237	$5s^25p^5\ ^2P^o_{3/2}$	$5s^25p^4(^3P)5d\ ^4D_{5/2}$	1.15E + 08	− 2.26
611.695	$5s^25p^5\ ^2P^o_{1/2}$	$5s^25p^4(^1D)5d\ ^2P_{1/2}$	4.52E + 07	− 2.66
617.600	$5s^25p^5\ ^2P^o_{1/2}$	$5s^25p^4(^3P)5d\ ^4P_{1/2}$	1.05E + 07	− 3.29
620.981	$5s^25p^5\ ^2P^o_{1/2}$	$5s^25p^4(^3P)5d\ ^4P_{3/2}$	3.28E + 07	− 2.79
675.154	$5s^25p^5\ ^2P^o_{1/2}$	$5s^25p^4(^3P)5d\ ^4D_{1/2}$	1.76E + 05	− 5.00
686.469	$5s^25p^5\ ^2P^o_{1/2}$	$5s^25p^4(^3P)5d\ ^4D_{3/2}$	2.56E + 05	− 4.70
699.449	$5s^25p^5\ ^2P^o_{3/2}$	$5s5p^6\ ^2S_{1/2}$	5.70E + 08	− 1.44
824.156	$5s^25p^5\ ^2P^o_{1/2}$	$5s5p^6\ ^2S_{1/2}$	3.53E + 08	− 1.52

[a]Epstein & Reader (1976); [b]HFR + CPOL calculations (this work).

were progressively considered by adding single and double (SD) excitations to an active set of orbitals, as summarized in Table 2.

Let us note that, for La V–IX, the orbitals 1s to 5p were optimized on the $5s^25p^k$ (k = 1–5) ground configuration, while the 4f and 5d orbitals were optimized using the MR configurations, keeping all other orbitals fixed. In the case of La X, the orbitals 1s to 5s were optimized on the $5s^2$ ground configuration, while the 5p, 5d, and 4f orbitals were optimized on the MR. In the VV steps, only the new orbitals were optimized, the other ones being kept to their values obtained before. Finally, from the latter calculation (VV3), a CV model was built by adding SD excitations from the 4d core orbital to the VV1 valence orbitals, namely 5s, 5p, 5d, 5f, and 5g. This model gave rise to rather large calculations since the total number of J-dependent configuration state functions (CSFs) varied from a few hundred thousand (La X) to over 4 million (La V) when considering the two parities together, as shown in Table 2.

Table 4. Transition probabilities (gA) and oscillator strengths ($\log gf$) for experimentally observed lines in La VI.

λ_{obs} (Å)[a]	Transition[a] Lower level	Upper level	gA (s^{-1})[b]	$\log gf$ [b]
335.648	$5s^25p^4\,^3P_1$	$5s^25p^36s\ 318315.7^o_2$	2.30E + 10	− 0.45
342.992	$5s^25p^4\,^1D_2$	$5s^25p^36s\ 320508.5^o_1$	2.69E + 10	− 0.36
343.921	$5s^25p^4\,^3P_2$	$5s^25p^36s\ 290764.4^o_2$	1.05E + 10	− 0.77
345.202	$5s^25p^4\,^3P_0$	$5s^25p^36s\ 302474.6^o_1$	2.54E + 10	− 0.39
345.589	$5s^25p^4\,^1D_2$	$5s^25p^36s\ 318315.7^o_2$	3.02E + 10	− 0.31
347.338	$5s^25p^4\,^3P_2$	$5s^25p^36s\ 287903.8^o_3$	7.08E + 10	0.07
354.488	$5s^25p^4\,^3P_1$	$5s^25p^36s\ 302474.6^o_1$	2.81E + 09	− 1.33
355.617	$5s^25p^4\,^3P_2$	$5s^25p^36s\ 281198.0^o_2$	3.84E + 10	− 0.18
365.605	$5s^25p^4\,^1D_2$	$5s^25p^36s\ 302474.6^o_1$	8.30E + 09	− 0.83
369.847	$5s^25p^4\,^3P_1$	$5s^25p^36s\ 290764.4^o_2$	1.02E + 10	− 0.72
370.037	$5s^25p^4\,^3P_0$	$5s^25p^36s\ 283029.4^o_1$	1.46E + 09	− 1.56
375.632	$5s^25p^4\,^3P_2$	$5s^25p^36s\ 266218.0^o_1$	5.56E + 10	0.03
380.739	$5s^25p^4\,^3P_1$	$5s^25p^36s\ 283029.4^o_1$	4.67E + 10	− 0.04
381.960	$5s^25p^4\,^1D_2$	$5s^25p^36s\ 290764.4^o_2$	1.06E + 11	0.32
383.423	$5s^25p^4\,^3P_1$	$5s^25p^36s\ 281198.0^o_2$	1.15E + 10	− 0.64
383.688	$5s^25p^4\,^1S_0$	$5s^25p^36s\ 320508.5^o_1$	4.31E + 10	− 0.07
384.427	$5s^25p^4\,^3P_2$	$5s^25p^36s\ 260127.8^o_2$	4.23E + 09	− 1.07
386.191	$5s^25p^4\,^1D_2$	$5s^25p^36s\ 287903.8^o_3$	9.93E + 09	− 0.70
387.591	$5s^25p^4\,^3P_2$	$5s^25p^35d\ 258004.7^o_1$	1.63E + 09	− 1.47
393.588	$5s^25p^4\,^1D_2$	$5s^25p^36s\ 283029.4^o_1$	3.81E + 09	− 1.10
394.585	$5s^25p^4\,^3P_0$	$5s^25p^36s\ 266218.0^o_1$	2.07E + 10	− 0.36
396.453	$5s^25p^4\,^1D_2$	$5s^25p^36s\ 281198.0^o_2$	6.57E + 09	− 0.86
399.283	$5s^25p^4\,^3P_2$	$5s^25p^35d\ 250443.6^o_2$	2.39E + 09	− 1.30
406.781	$5s^25p^4\,^3P_1$	$5s^25p^36s\ 266218.0^o_1$	2.07E + 10	− 0.34
407.208	$5s^25p^4\,^3P_2$	$5s^25p^35d\ 245575.7^o_2$	4.27E + 09	− 0.96
407.799	$5s^25p^4\,^3P_0$	$5s^25p^35d\ 258004.7^o_1$	1.29E + 11	0.47
410.350	$5s^25p^4\,^3P_1$	$5s^25p^35d\ 264077.8^o_2$	2.15E + 11	0.17
412.210	$5s^25p^4\,^3P_2$	$5s^25p^35d\ 242595.3^o_1$	6.62E + 09	− 0.89
412.210	$5s^25p^4\,^1S_0$	$5s^25p^36s\ 302474.6^o_1$	8.84E + 09	− 0.71
414.875	$5s^25p^4\,^3P_2$	$5s^25p^35d\ 241036.5^o_3$	4.38E + 11	0.99
419.153	$5s^25p^4\,^3P_0$	$5s^25p^35d\ 251363.6^o_1$	4.66E + 10	0.05
419.226	$5s^25p^4\,^3P_2$	$5s^25p^35d\ 238534.7^o_1$	8.98E + 10	0.32
419.557	$5s^25p^4\,^1D_2$	$5s^25p^35d\ 267303.0^o_3$	1.42E + 09	− 1.47
420.836	$5s^25p^4\,^3P_1$	$5s^25p^35d\ 258004.7^o_1$	5.24E + 10	0.07
422.414	$5s^25p^4\,^3P_2$	$5s^25p^35d\ 236734.2^o_2$	7.40E + 10	0.24
425.311	$5s^25p^4\,^1D_2$	$5s^25p^35d\ 264077.8^o_2$	5.59E + 10	0.16
425.562	$5s^25p^4\,^3P_1$	$5s^25p^35d\ 255365.8^o_0$	5.57E + 10	0.10
428.291	$5s^25p^4\,^3P_2$	$5s^25p^35d\ 233486.4^o_3$	2.46E + 10	− 0.21
430.356	$5s^25p^4\,^3P_2$	$5s^25p^35d\ 232365.7^o_3$	8.58E + 09	− 0.66
430.761	$5s^25p^4\,^3P_2$	$5s^25p^35d\ 232147.9^o_2$	7.50E + 08	− 1.70
432.940	$5s^25p^4\,^3P_1$	$5s^25p^35d\ 251363.3^o_1$	5.24E + 10	0.07
434.667	$5s^25p^4\,^3P_1$	$5s^25p^35d\ 250443.6^o_2$	2.15E + 11	0.72
435.141	$5s^25p^4\,^3P_0$	$5s^25p^35d\ 242595.3^o_1$	4.66E + 10	0.05
436.587	$5s^25p^4\,^1D_2$	$5s^25p^35d\ 258004.7^o_1$	6.58E + 10	0.20
438.011	$5s^25p^4\,^3P_2$	$5s^25p^35d\ 228302.7^o_2$	2.10E + 09	− 1.18
444.060	$5s^25p^4\,^3P_1$	$5s^25p^35d\ 245575.7^o_2$	1.06E + 10	− 0.50
444.839	$5s^25p^4\,^3P_2$	$5s^25p^35d\ 224798.4^o_1$	1.06E + 10	− 0.55
448.136	$5s^25p^4\,^1S_0$	$5s^25p^36s\ 283029.4^o_1$	3.79E + 08	− 2.00
449.627	$5s^25p^4\,^1D_2$	$5s^25p^35d\ 251363.3^o_1$	2.46E + 10	− 0.20
450.020	$5s^25p^4\,^3P_1$	$5s^25p^35d\ 242595.3^o_1$	3.83E + 10	− 0.02
451.337	$5s^25p^4\,^3P_2$	$5s^25p^35d\ 221564.0^o_2$	3.38E + 09	− 1.02
451.494	$5s^25p^4\,^1D_2$	$5s^25p^35d\ 250443.6^o_2$	5.59E + 10	0.16
461.640	$5s^25p^4\,^1D_2$	$5s^25p^35d\ 245575.7^o_2$	4.75E + 09	− 0.81
462.215	$5s^25p^4\,^3P_1$	$5s^25p^35d\ 236734.2^o_2$	2.45E + 06	− 4.00
465.210	$5s^25p^4\,^3P_2$	$5s^25p^35d\ 214956.5^o_1$	2.29E + 08	− 2.17
468.080	$5s^25p^4\,^1D_2$	$5s^25p^35d\ 242595.3^o_1$	3.33E + 10	− 0.04
471.517	$5s^25p^4\,^1D_2$	$5s^25p^35d\ 241036.5^o_3$	3.10E + 08	− 2.05
472.220	$5s^25p^4\,^3P_1$	$5s^25p^35d\ 232147.9^o_2$	2.10E + 09	− 1.18
477.146	$5s^25p^4\,^1D_2$	$5s^25p^35d\ 238534.7^o_1$	1.05E + 10	− 0.51
480.956	$5s^25p^4\,^3P_1$	$5s^25p^35d\ 228302.7^o_2$	2.10E + 09	− 1.18
481.283	$5s^25p^4\,^1D_2$	$5s^25p^35d\ 236734.2^o_2$	5.40E + 09	− 0.79
484.902	$5s^25p^4\,^3P_2$	$5s^25p^35d\ 206227.2^o_3$	5.74E + 09	− 0.74

Table 4 – *continued*

λ_{obs} (Å)[a]	Transition[a] Lower level	Upper level	gA (s^{-1})[b]	log gf [b]
486.399	$5s^25p^4\ ^3P_1$	$5s^25p^35d\ 225975.1^o_0$	1.32E + 09	− 1.38
488.925	$5s^25p^4\ ^1D_2$	$5s^25p^35d\ 233486.4^o_3$	5.70E + 09	− 0.74
489.204	$5s^25p^4\ ^3P_1$	$5s^25p^35d\ 224798.4^o_1$	4.69E + 09	− 0.83
489.281	$5s^25p^4\ ^3P_2$	$5s^25p^35d\ 204381.5^o_3$	2.44E + 09	− 1.10
491.620	$5s^25p^4\ ^1D_2$	$5s^25p^35d\ 232365.7^o_3$	5.91E + 09	− 0.71
492.146	$5s^25p^4\ ^1D_2$	$5s^25p^35d\ 232147.9^o_2$	4.56E + 07	− 2.81
494.638	$5s^25p^4\ ^3P_0$	$5s^25p^35d\ 214956.5^o_1$	6.02E + 09	− 0.71
495.491	$5s^25p^4\ ^3P_2$	$5s^25p^35d\ 201819.9^o_2$	1.54E + 09	− 1.29
497.065	$5s^25p^4\ ^3P_1$	$5s^25p^35d\ 221564.0^o_2$	6.06E + 08	− 1.70
500.106	$5s^25p^4\ ^3P_2$	$5s^25p^35d\ 199957.4^o_1$	4.63E + 08	− 1.81
503.396	$5s^25p^4\ ^3P_2$	$5s^25p^35d\ 198650.7^o_3$	1.76E + 09	− 1.22
504.738	$5s^25p^4\ ^1S_0$	$5s^25p^35d\ 258004.7^o_1$	8.09E + 08	− 1.57
510.616	$5s^25p^4\ ^1D_2$	$5s^25p^35d\ 224798.4^o_1$	1.26E + 09	− 1.36
519.189	$5s^25p^4\ ^1D_2$	$5s^25p^35d\ 221564.0^o_2$	8.96E + 08	− 1.49
522.231	$5s^25p^4\ ^1S_0$	$5s^25p^35d\ 251363.3^o_1$	3.17E + 08	− 1.95
526.578	$5s^25p^4\ ^3P_2$	$5s^25p^35d\ 189905.4^o_2$	2.35E + 09	− 1.05
534.275	$5s^25p^4\ ^3P_0$	$5s^25p^35d\ 199957.4^o_1$	4.38E + 08	− 1.77
537.632	$5s^25p^4\ ^1D_2$	$5s^25p^35d\ 214956.5^o_1$	8.15E + 08	− 1.51
539.480	$5s^25p^4\ ^3P_2$	$5s5p^5\ 185363.7^o_1$	1.07E + 09	− 1.37
545.351	$5s^25p^4\ ^3P_2$	$5s^25p^35d\ 183366.3^o_1$	3.83E + 08	− 1.81
548.515	$5s^25p^4\ ^3P_2$	$5s^25p^35d\ 182310.1^o_3$	9.65E + 08	− 1.40
549.237	$5s^25p^4\ ^3P_2$	$5s^25p^35d\ 182070.9^o_2$	9.63E + 08	− 1.40
564.108	$5s^25p^4\ ^1D_2$	$5s^25p^35d\ 206227.2^o_3$	4.58E + 08	− 1.71
570.044	$5s^25p^4\ ^1D_2$	$5s^25p^35d\ 204381.5^o_3$	1.29E + 08	− 2.25
586.239	$5s^25p^4\ ^3P_0$	$5s^25p^35d\ 183366.3^o_1$	1.22E + 08	− 2.24
613.559	$5s^25p^4\ ^3P_1$	$5s^25p^35d\ 183366.3^o_1$	2.93E + 08	− 1.83
615.372	$5s^25p^4\ ^3P_1$	$5s^25p^35d\ 182885.9^o_0$	2.40E + 08	− 1.92
621.313	$5s^25p^4\ ^1D_2$	$5s^25p^35d\ 189905.4^o_2$	6.15E + 07	− 2.50
637.640	$5s^25p^4\ ^3P_2$	$5s5p^5\ 156828.3^o_1$	1.49E + 09	− 1.08
639.357	$5s^25p^4\ ^1D_2$	$5s5p^5\ 185363.7^o_1$	3.06E + 09	− 0.78
647.629	$5s^25p^4\ ^1D_2$	$5s^25p^35d\ 183366.3^o_1$	6.48E + 08	− 1.44
652.092	$5s^25p^4\ ^1D_2$	$5s^25p^35d\ 182310.1^o_3$	1.04E + 07	− 3.23
675.903	$5s^25p^4\ ^3P_1$	$5s5p^5\ 168332.8^o_0$	6.69E + 08	− 1.38
681.484	$5s^25p^4\ ^3P_2$	$5s5p^5\ 146738.0^o_2$	2.35E + 09	− 0.83
694.244	$5s^25p^4\ ^3P_0$	$5s5p^5\ 156828.3^o_1$	6.28E + 08	− 1.39
732.891	$5s^25p^4\ ^3P_1$	$5s5p^5\ 156828.3^o_1$	4.65E + 08	− 1.48
782.041	$5s^25p^4\ ^1D_2$	$5s5p^5\ 156828.3^o_1$	1.91E + 08	− 1.81
791.422	$5s^25p^4\ ^3P_1$	$5s5p^5\ 146738.0^o_2$	8.87E + 08	− 1.14
796.915	$5s^25p^4\ ^1S_0$	$5s5p^5\ 185363.7^o_1$	2.34E + 08	− 1.72
849.028	$5s^25p^4\ ^1D_2$	$5s5p^5\ 146738.0^o_2$	3.79E + 08	− 1.45
1031.476	$5s^25p^4\ ^1S_0$	$5s5p^5\ 156828.3^o_1$	3.43E + 07	− 2.34

[a]Gayasov et al. (1997); [b]HFR + CPOL calculations (this work).

A comparison of our MCDHF energy level values obtained in CV models with available experimental energy levels revealed a good agreement, the mean deviation $\Delta E/E_{Exp}$ (with $\Delta E = E_{MCDHF} - E_{Exp}$) being found to be equal to 0.016 ± 0.005 (La V), 0.012 ± 0.019 (La VI), 0.020 ± 0.014 (La VII), −0.003 ± 0.021 (La VIII), −0.001 ± 0.011 (La IX), and 0.048 ± 0.050 (La X) when considering the experimental data reported by Epstein & Reader (1976), Gayasov et al. (1997, 1998), Gayasov & Joshi (1998), Churilov & Joshi (2001), Ryabtsev et al. (2002), and Tauheed et al. (2008).

3.3 AMBiT code

The PH-CI method (Berengut 2016) as implemented in the AMBiT atomic structure code (Kahl & Berengut 2019) was used in order to calculate the level energies and radiative parameters in three representative lanthanum ions, i.e. La V, La VIII, and La X. Moreover, the emu CI approximation (Geddes et al. 2018) as coded in the AMBiT program was further employed so to reduce the size of the problem without losing much accuracy. These fully relativistic approaches were described in details in our previous study dedicated to the Ce V–X ions (Carvajal Gallego et al. 2022) and will not be repeated here.

Our AMBiT calculations were focused on the properties of the experimental energy levels found in the literature. These levels are the following: 31 levels of La V belonging to the configurations $5s^25p^5$, $5s5p^6$, $5s^25p^45d$, and $5s^25p^46s$ with symmetries $J^\Pi = 1/2^{even}$–$5/2^{even}$, $1/2^{odd}$–$3/2^{odd}$ determined by Epstein & Reader (1976), 31 levels of La VIII reported by Tauheed et al. (2008) and belonging to the configurations $5s^25p^2$, $5s5p^3$, $5s^25p5d$, and $5s^25p6s$ with symmetries $J^\Pi = 0^{even}$–2^{even}, 0^{odd}–3^{odd}, and 63 levels of La X published by Ryabtsev et al. (2002) and belonging to the configurations $5s^2$, 5s5p, 5s6p, 5s4f, 5s5f, 5s5d, 5s6s, $5p^2$, 5p4f, 5p5d, and 4f5d with symmetries $J^\Pi = 0^{even}$–5^{even}, 0^{odd}–6^{odd}. But, the two $4d^95s^25p$ levels with $J^\Pi = 1^{odd}$ reported by Kaufman & Sugar (1987) for La X were

Table 5. Transition probabilities (gA) and oscillator strengths ($\log gf$) for experimentally observed lines in La VII.

λ_{obs} (Å)[a]	Transition[a]		gA (s^{-1})[b]	$\log gf$[b]
	Lower level	Upper level		
307.150	$5s^25p^3\ ^2D^o_{3/2}$	$5s^25p^26s\ 345450.0_{5/2}$	3.23E + 10	− 0.37
308.473	$5s^25p^3\ ^4S^o_{3/2}$	$5s^25p^26s\ 324181.0_{3/2}$	7.91E + 09	− 0.98
310.991	$5s^25p^3\ ^2D^o_{5/2}$	$5s^25p^26s\ 348538.0_{3/2}$	1.92E + 10	− 0.59
311.627	$5s^25p^3\ ^4S^o_{3/2}$	$5s^25p^26s\ 320896.3_{5/2}$	6.53E + 10	− 0.05
313.553	$5s^25p^3\ ^4S^o_{3/2}$	$5s^25p^26s\ 318923.0_{1/2}$	5.56E + 09	− 1.12
314.007	$5s^25p^3\ ^2D^o_{5/2}$	$5s^25p^26s\ 345450.0_{5/2}$	5.98E + 10	− 0.08
318.237	$5s^25p^3\ ^4S^o_{3/2}$	$5s^25p^26s\ 314222.0_{3/2}$	2.45E + 10	− 0.46
328.609	$5s^25p^3\ ^2D^o_{3/2}$	$5s^25p^26s\ 324181.0_{3/2}$	1.77E + 10	− 0.58
334.395	$5s^25p^3\ ^2D^o_{3/2}$	$5s^25p^26s\ 318923.0_{1/2}$	4.77E + 10	− 0.13
336.491	$5s^25p^3\ ^2D^o_{5/2}$	$5s^25p^26s\ 324181.0_{5/2}$	7.32E + 10	0.06
337.143	$5s^25p^3\ ^4S^o_{3/2}$	$5s^25p^26s\ 296609.8_{1/2}$	2.08E + 10	− 0.48
339.738	$5s^25p^3\ ^2D^o_{3/2}$	$5s^25p^26s\ 314222.0_{3/2}$	3.75E + 09	− 1.22
340.255	$5s^25p^3\ ^2D^o_{5/2}$	$5s^25p^26s\ 320896.3_{5/2}$	2.45E + 10	− 0.40
343.848	$5s^25p^3\ ^2P^o_{3/2}$	$5s^25p^26s\ 348538.0_{3/2}$	7.20E + 10	0.07
347.540	$5s^25p^3\ ^2P^o_{3/2}$	$5s^25p^26s\ 345450.0_{5/2}$	1.87E + 10	− 0.51
348.164	$5s^25p^3\ ^2D^o_{5/2}$	$5s^25p^26s\ 314222.0_{3/2}$	7.11E + 09	− 0.92
352.745	$5s^25p^3\ ^2P^o_{1/2}$	$5s^25p^26s\ 324181.0_{3/2}$	3.66E + 10	− 0.20
359.410	$5s^25p^3\ ^2P^o_{1/2}$	$5s^25p^26s\ 318923.0_{1/2}$	1.88E + 10	− 0.47
378.933	$5s^25p^3\ ^2D^o_{5/2}$	$5s^25p^25d\ 290890.7_{5/2}$	6.98E + 08	− 1.86
379.949	$5s^25p^3\ ^2P^o_{3/2}$	$5s^25p^26s\ 320896.3_{5/2}$	1.61E + 09	− 1.50
390.528	$5s^25p^3\ ^4S^o_{3/2}$	$5s^25p^25d\ 256064.4_{5/2}$	3.82E + 10	− 0.11
397.462	$5s^25p^3\ ^4S^o_{3/2}$	$5s^25p^25d\ 251595.7_{3/2}$	5.37E + 10	0.07
401.619	$5s^25p^3\ ^2P^o_{1/2}$	$5s^25p^25d\ 289686.6_{3/2}$	7.59E + 10	0.22
403.228	$5s^25p^3\ ^2D^o_{5/2}$	$5s^25p^25d\ 274989.8_{5/2}$	1.68E + 10	− 0.40
407.895	$5s^25p^3\ ^2D^o_{5/2}$	$5s^25p^25d\ 272152.3_{7/2}$	2.71E + 11	0.77
408.263	$5s^25p^3\ ^4S^o_{3/2}$	$5s^25p^25d\ 244939.9_{1/2}$	9.46E + 10	0.32
410.550	$5s^25p^3\ ^4S^o_{3/2}$	$5s^25p^25d\ 243575.9_{3/2}$	1.08E + 11	0.39
411.113	$5s^25p^3\ ^2D^o_{3/2}$	$5s^25p^25d\ 263111.5_{5/2}$	4.66E + 10	0.01
412.045	$5s^25p^3\ ^2D^o_{3/2}$	$5s^25p^25d\ 262560.6_{3/2}$	1.01E + 10	− 0.68
412.389	$5s^25p^3\ ^2D^o_{3/2}$	$5s^25p^25d\ 262358.0_{1/2}$	5.98E + 08	− 1.86
414.949	$5s^25p^3\ ^4S^o_{3/2}$	$5s^25p^25d\ 240993.5_{5/2}$	2.33E + 11	0.73
420.550	$5s^25p^3\ ^4S^o_{3/2}$	$5s5p^4\ 237784.9_{3/2}$	4.88E + 09	− 0.86
421.545	$5s^25p^3\ ^2D^o_{3/2}$	$5s5p^4\ 257090.8_{1/2}$	5.69E + 10	0.13
423.376	$5s^25p^3\ ^2D^o_{3/2}$	$5s^25p^25d\ 256064.4_{5/2}$	6.73E + 10	0.20
423.511	$5s^25p^3\ ^2D^o_{5/2}$	$5s^25p^25d\ 263111.5_{5/2}$	6.98E + 10	0.20
424.503	$5s^25p^3\ ^2D^o_{5/2}$	$5s^25p^25d\ 262560.6_{3/2}$	9.38E + 07	− 2.69
428.858	$5s^25p^3\ ^2P^o_{3/2}$	$5s^25p^25d\ 290890.7_{5/2}$	1.22E + 11	0.48
431.082	$5s^25p^3\ ^2P^o_{3/2}$	$5s^25p^25d\ 289686.6_{3/2}$	2.08E + 10	− 0.28
436.537	$5s^25p^3\ ^2D^o_{5/2}$	$5s^25p^25d\ 256064.4_{5/2}$	9.41E + 10	0.38
438.915	$5s^25p^3\ ^4S^o_{3/2}$	$5s^25p^25d\ 227834.4_{5/2}$	1.11E + 10	− 0.52
445.236	$5s^25p^3\ ^2D^o_{5/2}$	$5s^25p^25d\ 251595.7_{3/2}$	1.35E + 10	− 0.44
447.006	$5s^25p^3\ ^2D^o_{3/2}$	$5s^25p^25d\ 243575.9_{3/2}$	1.61E + 10	− 0.37
450.479	$5s^25p^3\ ^4S^o_{3/2}$	$5s^25p^25d\ 221987.9_{3/2}$	4.88E + 09	− 0.86
450.727	$5s^25p^3\ ^2P^o_{1/2}$	$5s^25p^25d\ 262560.6_{3/2}$	3.92E + 10	− 0.03
451.140	$5s^25p^3\ ^2P^o_{1/2}$	$5s^25p^25d\ 262358.0_{1/2}$	5.06E + 10	0.14
452.233	$5s^25p^3\ ^2D^o_{3/2}$	$5s^25p^25d\ 240993.5_{5/2}$	1.71E + 10	− 0.33
454.503	$5s^25p^3\ ^2D^o_{5/2}$	$5s^25p^25d\ 247011.8_{7/2}$	6.23E + 09	− 0.74
458.894	$5s^25p^3\ ^2D^o_{3/2}$	$5s5p^4\ 237784.9_{3/2}$	4.41E + 10	0.09
461.712	$5s^25p^3\ ^2D^o_{5/2}$	$5s^25p^25d\ 243575.9_{3/2}$	2.91E + 10	− 0.08
462.119	$5s^25p^3\ ^2P^o_{1/2}$	$5s5p^4\ 257090.8_{1/2}$	8.04E + 09	− 0.65
464.837	$5s^25p^3\ ^4S^o_{3/2}$	$5s^25p^25d\ 215130.0_{5/2}$	2.87E + 09	− 1.06
467.283	$5s^25p^3\ ^2D^o_{5/2}$	$5s^25p^25d\ 240993.5_{5/2}$	1.54E + 10	− 0.35
469.949	$5s^25p^3\ ^2D^o_{5/2}$	$5s^25p^25d\ 239780.2_{7/2}$	1.12E + 10	− 0.46
474.158	$5s^25p^3\ ^2P^o_{1/2}$	$5s^25p^25d\ 251595.7_{3/2}$	5.40E + 09	− 0.79
474.395	$5s^25p^3\ ^2D^o_{5/2}$	$5s5p^4\ 237784.9_{3/2}$	5.10E + 09	− 0.62
480.843	$5s^25p^3\ ^2D^o_{3/2}$	$5s^25p^25d\ 227834.4_{5/2}$	3.83E + 09	− 0.91
483.627	$5s^25p^3\ ^2D^o_{3/2}$	$5s^25p^25d\ 226638.4_{1/2}$	2.27E + 09	− 1.12

Table 5 – *continued*

λ_{obs} (Å)^a	Transition^a		gA (s^{-1})^b	log gf ^{b}
	Lower level	Upper level		
485.238	$5s^25p^3\ ^4S^o_{3/2}$	$5s^25p^25d$ 206084.9$_{5/2}$	6.98E + 09	– 0.64
494.638	$5s^25p^3\ ^4S^o_{3/2}$	$5s^25p^25d$ 202171.9$_{3/2}$	2.18E + 09	– 1.13
494.751	$5s^25p^3\ ^2D^o_{3/2}$	$5s^25p^25d$ 221987.9$_{3/2}$	9.14E + 08	– 1.51
497.901	$5s^25p^3\ ^2D^o_{5/2}$	$5s^25p^25d$ 227834.4$_{5/2}$	3.88E + 09	– 0.87
500.106	$5s^25p^3\ ^4S^o_{3/2}$	$5s5p^4$ 199957.0$_{1/2}$	1.09E + 09	– 1.42
501.559	$5s^25p^3\ ^2P^o_{3/2}$	$5s5p^4$ 257090.8$_{1/2}$	7.52E + 09	– 0.61
504.210	$5s^25p^3\ ^2D^o_{3/2}$	$5s^25p^25d$ 218195.0$_{1/2}$	6.91E + 08	– 1.61
505.704	$5s^25p^3\ ^4S^o_{3/2}$	$5s^25p^25d$ 197741.4$_{3/2}$	2.41E + 08	– 2.06
512.826	$5s^25p^3\ ^2D^o_{5/2}$	$5s^25p^25d$ 221987.9$_{3/2}$	5.15E + 09	– 0.72
531.518	$5s^25p^3\ ^2D^o_{5/2}$	$5s^25p^25d$ 215130.0$_{5/2}$	1.22E + 08	– 2.32
537.007	$5s^25p^3\ ^2D^o_{3/2}$	$5s^25p^25d$ 206084.9$_{5/2}$	2.78E + 08	– 1.95
545.705	$5s^25p^3\ ^4S^o_{3/2}$	$5s5p^4$ 183252.2$_{5/2}$	7.62E + 07	– 2.49
548.514	$5s^25p^3\ ^2D^o_{3/2}$	$5s^25p^25d$ 202171.9$_{3/2}$	1.51E + 09	– 1.20
551.608	$5s^25p^3\ ^2P^o_{1/2}$	$5s^25p^25d$ 221987.9$_{3/2}$	2.37E + 08	– 2.00
555.264	$5s^25p^3\ ^2D^o_{3/2}$	$5s5p^4$ 199957.0$_{1/2}$	4.90E + 09	– 0.68
558.366	$5s^25p^3\ ^2D^o_{5/2}$	$5s^25p^25d$ 206084.9$_{5/2}$	4.42E + 08	– 1.72
562.201	$5s^25p^3\ ^2D^o_{3/2}$	$5s^25p^25d$ 197741.4$_{3/2}$	1.50E + 08	– 2.18
563.387	$5s^25p^3\ ^2P^o_{1/2}$	$5s^25p^25d$ 218195.0$_{1/2}$	6.45E + 08	– 1.54
565.820	$5s^25p^3\ ^4S^o_{3/2}$	$5s5p^4$ 176734.1$_{3/2}$	5.54E + 08	– 1.60
570.840	$5s^25p^3\ ^2D^o_{5/2}$	$5s^25p^25d$ 202171.9$_{3/2}$	4.59E + 09	– 0.68
585.655	$5s^25p^3\ ^2D^o_{5/2}$	$5s^25p^25d$ 197741.4$_{3/2}$	5.10E + 09	– 0.62
591.969	$5s^25p^3\ ^2P^o_{3/2}$	$5s^25p^25d$ 226638.4$_{1/2}$	3.54E + 09	– 0.77
608.732	$5s^25p^3\ ^2P^o_{3/2}$	$5s^25p^25d$ 221987.9$_{3/2}$	2.29E + 08	– 1.94
612.043	$5s^25p^3\ ^2D^o_{3/2}$	$5s5p^4$ 183252.2$_{5/2}$	1.34E + 07	– 3.15
619.281	$5s^25p^3\ ^2P^o_{1/2}$	$5s^25p^25d$ 202171.9$_{3/2}$	5.20E + 07	– 2.56
623.136	$5s^25p^3\ ^2P^o_{3/2}$	$5s^25p^25d$ 218195.0$_{1/2}$	6.20E + 08	– 1.49
623.935	$5s^25p^3\ ^4S^o_{3/2}$	$5s5p^4$ 160273.2$_{1/2}$	1.68E + 09	– 1.03
627.906	$5s^25p^3\ ^2P^o_{1/2}$	$5s5p^4$ 199957.0$_{1/2}$	2.26E + 09	– 0.92
636.341	$5s^25p^3\ ^4S^o_{3/2}$	$5s5p^4$ 157148.5$_{3/2}$	3.32E + 09	– 0.71
636.763	$5s^25p^3\ ^2P^o_{1/2}$	$5s^25p^25d$ 197741.4$_{3/2}$	8.73E + 08	– 1.31
637.490	$5s^25p^3\ ^2D^o_{3/2}$	$5s5p^4$ 176734.1$_{3/2}$	5.57E + 09	– 0.50
639.956	$5s^25p^3\ ^2D^o_{5/2}$	$5s5p^4$ 183252.2$_{5/2}$	5.63E + 09	– 0.48
667.813	$5s^25p^3\ ^2D^o_{5/2}$	$5s5p^4$ 176734.1$_{3/2}$	2.41E + 08	– 1.82
692.227	$5s^25p^3\ ^2P^o_{3/2}$	$5s^25p^25d$ 202171.9$_{3/2}$	3.01E + 08	– 1.71
697.596	$5s^25p^3\ ^4S^o_{3/2}$	$5s5p^4$ 143349.5$_{5/2}$	2.77E + 09	– 0.72
703.005	$5s^25p^3\ ^2P^o_{3/2}$	$5s5p^4$ 199957.0$_{1/2}$	1.26E + 08	– 2.08
712.219	$5s^25p^3\ ^2D^o_{3/2}$	$5s5p^4$ 160273.2$_{1/2}$	7.97E + 07	– 2.24
728.439	$5s^25p^3\ ^2D^o_{3/2}$	$5s5p^4$ 157148.5$_{3/2}$	1.16E + 06	– 4.05
735.096	$5s^25p^3\ ^2P^o_{1/2}$	$5s5p^4$ 176734.1$_{3/2}$	2.31E + 08	– 1.76
768.302	$5s^25p^3\ ^2D^o_{5/2}$	$5s5p^4$ 157148.5$_{3/2}$	1.79E + 08	– 1.83
796.540	$5s^25p^3\ ^2P^o_{3/2}$	$5s5p^4$ 183252.2$_{5/2}$	1.55E + 09	– 0.87
809.841	$5s^25p^3\ ^2D^o_{3/2}$	$5s5p^4$ 143349.5$_{5/2}$	7.04E + 08	– 1.19
836.288	$5s^25p^3\ ^2P^o_{1/2}$	$5s5p^4$ 160273.2$_{1/2}$	1.28E + 08	– 1.90
859.416	$5s^25p^3\ ^2D^o_{5/2}$	$5s5p^4$ 143349.5$_{5/2}$	3.47E + 08	– 1.44
975.027	$5s^25p^3\ ^2P^o_{3/2}$	$5s5p^4$ 160273.2$_{1/2}$	1.32E + 07	– 2.77
1005.649	$5s^25p^3\ ^2P^o_{3/2}$	$5s5p^4$ 157148.5$_{3/2}$	7.44E + 07	– 1.99

[a]Gayasov et al. (1998); [b]HFR + CPOL calculations (this work).

not considered here as they were not confirmed neither by Gayasov et al. (1999) nor by Ryabtsev et al. (2002).

In order to carry out these calculations, different computational strategies were followed for the three ions. In La V, the core spin–orbitals and the frozen core potential $V^{N_{\rm core}}(r)$ were generated by solving the Dirac–Hartree–Fock (DHF) equations for the Cd-like ground configurations [Pd]5s^2 consisting in 48 electrons. The Breit and Quantum Electro-Dynamics (QED) interactions were included. The valence orbitals were determined by diagonalizing a set of B-splines using the DHF Hamiltonian with the above-mentioned frozen core potential. The emu CI expansions with symmetries $J^\Pi = 1/2^{\rm even}$–$5/2^{\rm even}$, $1/2^{\rm odd}$–$3/2^{\rm odd}$ were obtained by considering for the large side the single and double electron and hole excitations from leading configurations 5p^5, 5s^{-1}5p^6, 5p^{4}4f, 5p^{4}5d, and 5p^{4}6s (hereafter nl^{-k} stands for k holes in the nl shell) to the active set of orbitals 12spdfg with all the core orbitals lower than 5s inactive, i.e. 5s to 12s, 5p to 12p, 5d to 12d, 4f to 12f, and 5g to 12g. For the small side, the active set of orbitals was reduced to 6spdfg, single and double electron only excitations were considered. The resulting emu CI matrix dimensions were $N = 3959\,094$ for the large side and

Table 6. Transition probabilities (gA) and oscillator strengths ($\log gf$) for experimentally observed lines in La VIII.

λ_{obs} (Å)[a]	Transition[a] Lower level	Upper level	gA (s^{-1})[b]	$\log gf$ [b]
280.260	$5s^25p^2\ ^3P_1$	$5s^25p6s\ ^3P^o_2$	2.80E + 10	− 0.50
284.336	$5s^25p^2\ ^3P_0$	$5s^25p6s\ ^3P^o_1$	3.28E + 10	− 0.41
285.384	$5s^25p^2\ ^3P_2$	$5s^25p6s\ ^3P^o_2$	4.72E + 10	− 0.26
302.277	$5s^25p^2\ ^3P_1$	$5s^25p6s\ ^3P^o_0$	2.55E + 10	− 0.47
303.414	$5s^25p^2\ ^1D_2$	$5s^25p6s\ ^1P^o_1$	7.85E + 10	0.01
306.767	$5s^25p^2\ ^3P_2$	$5s^25p6s\ ^3P^o_1$	5.57E + 10	− 0.12
307.321	$5s^25p^2\ ^1D_2$	$5s^25p6s\ ^3P^o_2$	3.07E + 10	− 0.39
322.811	$5s^25p^2\ ^1S_0$	$5s^25p6s\ ^1P^o_1$	1.48E + 10	− 0.66
370.024	$5s^25p^2\ ^3P_0$	$5s^25p5d\ 270253^o_1$	4.21E + 08	− 2.10
379.061	$5s^25p^2\ ^3P_2$	$5s^25p5d\ 289537^o_3$	2.00E + 10	− 0.41
391.082	$5s^25p^2\ ^3P_1$	$5s^25p5d\ 275025^o_1$	4.34E + 09	− 1.11
395.969	$5s^25p^2\ ^3P_1$	$5s^25p5d\ 271866^o_0$	2.89E + 10	− 0.20
398.509	$5s^25p^2\ ^3P_1$	$5s^25p5d\ 270253^o_1$	5.09E + 10	0.04
400.709	$5s^25p^2\ ^3P_1$	$5s^25p5d\ 268878^o_2$	1.66E + 10	− 0.44
401.128	$5s^25p^2\ ^3P_2$	$5s^25p5d\ 275025^o_1$	1.71E + 10	− 0.41
401.290	$5s^25p^2\ ^3P_0$	$5s^25p5d\ 249196^o_1$	3.75E + 10	− 0.07
401.373	$5s^25p^2\ ^3P_2$	$5s^25p5d\ 274872^o_2$	4.19E + 10	− 0.02
407.895	$5s^25p^2\ ^3P_2$	$5s^25p5d\ 270890^o_3$	1.81E + 11	0.62
408.095	$5s^25p^2\ ^3P_0$	$5s^25p5d\ 245042^o_1$	7.93E + 09	− 0.73
408.959	$5s^25p^2\ ^3P_2$	$5s^25p5d\ 270253^o_1$	3.37E + 09	− 1.08
411.267	$5s^25p^2\ ^3P_2$	$5s^25p5d\ 268878^o_2$	5.11E + 07	− 2.82
418.762	$5s^25p^2\ ^1D_2$	$5s^25p5d\ 289537^o_3$	4.92E + 10	0.05
435.017	$5s^25p^2\ ^3P_1$	$5s^25p5d\ 249196^o_1$	1.46E + 10	− 0.42
438.465	$5s^25p^2\ ^3P_1$	$5s^25p5d\ 247389^o_2$	5.52E + 10	0.17
443.030	$5s^25p^2\ ^3P_1$	$5s5p^3\ 245042^o_1$	1.02E + 10	− 0.56
445.851	$5s^25p^2\ ^1D_2$	$5s^25p5d\ 275025^o_1$	1.41E + 10	− 0.41
446.161	$5s^25p^2\ ^1D_2$	$5s^25p5d\ 274872^o_2$	2.64E + 10	− 0.14
451.140	$5s^25p^2\ ^3P_2$	$5s^25p5d\ 247389^o_2$	1.67E + 10	− 0.33
454.230	$5s^25p^2\ ^1D_2$	$5s^25p5d\ 270890^o_3$	2.31E + 10	− 0.19
455.551	$5s^25p^2\ ^1D_2$	$5s^25p5d\ 270253^o_1$	1.88E + 09	− 1.38
455.956	$5s^25p^2\ ^3P_2$	$5s5p^3\ 245042^o_1$	5.18E + 08	− 1.83
458.423	$5s^25p^2\ ^1D_2$	$5s^25p5d\ 268878^o_2$	3.17E + 10	− 0.04
459.727	$5s^25p^2\ ^3P_0$	$5s5p^3\ 217519^o_1$	1.12E + 10	− 0.49
466.767	$5s^25p^2\ ^3P_2$	$5s^25p5d\ 239969^o_3$	2.94E + 09	− 1.00
477.454	$5s^25p^2\ ^3P_1$	$5s^25p5d\ 228766^o_2$	2.02E + 09	− 1.18
479.129	$5s^25p^2\ ^3P_2$	$5s5p^24f\ 234437^o_3$	1.35E + 10	− 0.37
489.046	$5s^25p^2\ ^1S_0$	$5s^25p5d\ 275025^o_1$	6.04E + 07	− 2.70
492.517	$5s^25p^2\ ^3P_2$	$5s^25p5d\ 228766^o_2$	3.99E + 09	− 0.86
503.887	$5s^25p^2\ ^1D_2$	$5s^25p5d\ 249196^o_1$	7.25E + 09	− 0.60
504.545	$5s^25p^2\ ^3P_1$	$5s^25p5d\ 217519^o_1$	1.93E + 10	− 0.18
507.156	$5s^25p^2\ ^3P_1$	$5s5p^3\ 216497^o_2$	4.24E + 08	− 1.79
508.511	$5s^25p^2\ ^1D_2$	$5s^25p5d\ 247389^o_2$	3.40E + 09	− 0.92
511.630	$5s^25p^2\ ^3P_0$	$5s5p^3\ 195453^o_1$	1.95E + 09	− 1.12
514.659	$5s^25p^2\ ^1D_2$	$5s5p^3\ 245042^o_1$	2.68E + 10	− 0.02
521.397	$5s^25p^2\ ^3P_2$	$5s5p^3\ 217519^o_1$	4.70E + 10	0.24
528.453	$5s^25p^2\ ^1D_2$	$5s^25p5d\ 239969^o_3$	1.05E + 08	− 2.38
544.375	$5s^25p^2\ ^1D_2$	$5s5p^24f\ 234437^o_3$	1.05E + 08	− 2.38
559.753	$5s^25p^2\ ^1S_0$	$5s^25p5d\ 249196^o_1$	2.03E + 08	− 2.07
561.708	$5s^25p^2\ ^1D_2$	$5s^25p5d\ 228766^o_2$	2.03E + 09	− 1.04
567.753	$5s^25p^2\ ^3P_1$	$5s5p^3\ 195453^o_1$	6.55E + 09	− 0.51
573.071	$5s^25p^2\ ^1S_0$	$5s5p^3\ 245042^o_1$	4.18E + 09	− 0.73
575.852	$5s^25p^2\ ^3P_1$	$5s5p^3\ 192976^o_0$	2.29E + 09	− 0.96
584.760	$5s^25p^2\ ^3P_2$	$5s5p^3\ 196738^o_2$	1.22E + 10	− 0.21
589.188	$5s^25p^2\ ^3P_2$	$5s5p^3\ 195453^o_1$	2.58E + 08	− 1.88
599.598	$5s^25p^2\ ^1D_2$	$5s5p^3\ 217519^o_1$	7.18E + 08	− 1.47
603.291	$5s^25p^2\ ^1D_2$	$5s5p^3\ 216497^o_2$	1.04E + 10	− 0.26
603.881	$5s^25p^2\ ^3P_0$	$5s5p^3\ 165594^o_1$	4.17E + 09	− 0.64
664.918	$5s^25p^2\ ^3P_2$	$5s5p^3\ 176121^o_3$	3.31E + 09	− 0.66
669.155	$5s^25p^2\ ^3P_1$	$5s5p^3\ 168764^o_2$	4.42E + 09	− 0.53
680.391	$5s^25p^2\ ^1S_0$	$5s5p^3\ 217519^o_1$	7.22E + 08	− 1.36
684.932	$5s^25p^2\ ^1D_2$	$5s5p^3\ 196738^o_2$	4.00E + 08	− 1.57
699.114	$5s^25p^2\ ^3P_2$	$5s5p^3\ 168764^o_2$	5.05E + 07	− 2.43

Table 6 – *continued*

λ_{obs} (Å)[a]	Transition[a] Lower level	Upper level	gA (s^{-1})[b]	log gf[b]
714.960	$5s^25p^2\ ^3P_2$	$5s5p^3\ 165594^o_1$	3.36E + 08	– 1.60
797.561	$5s^25p^2\ ^1D_2$	$5s5p^3\ 176121^o_3$	1.84E + 09	– 0.76
800.581	$5s^25p^2\ ^1S_0$	$5s5p^3\ 195453^o_1$	1.79E + 08	– 1.78
842.378	$5s^25p^2\ ^3P_1$	$5s5p^3\ 138032^o_2$	2.34E + 08	– 1.60
847.275	$5s^25p^2\ ^1D_2$	$5s5p^3\ 168764^o_2$	7.66E + 07	– 2.10
870.654	$5s^25p^2\ ^1D_2$	$5s5p^3\ 165594^o_1$	1.21E + 08	– 1.88
890.432	$5s^25p^2\ ^3P_2$	$5s5p^3\ 138032^o_2$	1.77E + 08	– 1.67
1052.091	$5s^25p^2\ ^1S_0$	$5s5p^3\ 165594^o_1$	1.53E + 07	– 2.62
1145.559	$5s^25p^2\ ^1D_2$	$5s5p^3\ 138032^o_2$	1.45E + 07	– 2.55

[a]Tauheed et al. (2008); [b]HFR + CPOL calculations (this work).

$N_{small} = 52\,571$ for the small side. The relative differences, $\Delta E = (E_{cal} - E_{exp})/E_{exp}$, with respect to the experimental energy levels published by Epstein & Reader (1976) ranged from less than −4 per cent to 3 per cent with an average of −0.4 per cent and a standard deviation of 1.4 per cent.

Regarding La VIII, the DHF equations were solved in a first step for the ground configuration of the Cd-like La X system, i.e. [Pd]$5s^2$, with 48 electrons in order to obtain the core orbitals. This enabled us to build in a second step the core electron potential $V^{N_{core}}(r)$ and to solve the frozen core DHF equations for the valence orbitals. In both steps, the Breit and QED corrections were included. In the emu CI step, the 57-electron wavefunction expansions with symmetries $J^\Pi = 0^{even}$–2^{even}, 0^{odd}–3^{odd} were generated by considering for the large side all the single and double electron and hole excitations from the $5p^2$ and $5s^{-1}5p^3$ leading configurations to the 22spdfg active set keeping all the core orbitals lower than 5s inactive. For the small side, the double electron and hole excitations were restricted to the 12spdfg active set. The corresponding dimensions were $N = 611\,676$ for the large side and $N_{small} = 424\,386$ for the small side. Here, the relative differences, ΔE, between our eigenvalues and the available experimental energy levels (Tauheed et al. 2008) ranged from −5 per cent to 4 per cent with an average of 0.05 per cent and a standard deviation of 2.4 per cent.

Finally, for La X, the strategy was similar to the one adopted for La VIII with the exceptions of the leading configurations and the multielectron wavefunction symmetries. These were, respectively, $5s^{-0}$, $5s^{-1}5p$, and $5s^{-1}4f$, $J^\Pi = 0^{even}$–5^{even}, 0^{odd}–6^{odd}. The emu CI large and small side dimensions were $N = 49\,763$ and $N_{small} = 34\,863$. The relative differences with the experimental level energies of Ryabtsev et al. (2002) ranged from −4 per cent to 2 per cent with an average of −0.6 per cent and a standard deviation of 1.1 per cent.

In each ion, the E1 line strengths, S, were calculated in the Babushkin gauge with photon frequencies $\omega = 0$ (i.e. in the non-relativistic limit) using our AMBiT models for the observed transitions reported by Epstein & Reader (1976), Tauheed et al. (2008), and Ryabtsev et al. (2002). The corresponding weighted oscillator strengths, gf, were determined afterward from the AMBiT S-values using the formula given below (Cowan 1981):

$$gf = 3.0376 \times 10^{-6}\, \sigma\, S, \quad (1)$$

where σ is the wavenumber in cm^{-1} of the E1 transition as deduced from the AMBiT eigenvalues and S is in astronomical unit (au).

4 RADIATIVE PARAMETERS

Of the three methods mentioned above, the HFR + CPOL method provided radiative data for the largest number of transitions in La V–X ions, which is an essential aspect for opacity estimation. Therefore, in Tables 3–8, we give the HFR + CPOL transition probabilities (gA) and oscillator strengths (log gf) for all experimentally observed lines published to date. These latter data were taken from the works of Epstein & Reader (1976) for La V, Gayasov et al. (1997) for La VI, Gayasov et al. (1998) for La VII, Tauheed et al. (2008) for La VIII, Gayasov et al. (1998) and Churilov & Joshi (2001) for La IX, and Ryabtsev et al. (2002) for La X. In Tables 7 and 8, we also list the gA values previously calculated by Churilov & Joshi (2001) and Ryabtsev et al. (2002) for La IX and La X, respectively. The comparison between these results and ours is illustrated in Fig. 2 where the ratio $gA_{HFR+CPOL}/gA_{Previous}$ is plotted as a function of $gA_{HFR+CPOL}$. When looking at this figure, we can notice that, while the overall agreement is relatively satisfactory, some notable discrepancies (larger than a factor of 2) are observed between the two sets of results, with average ratios of 0.800 ± 0.756 and 0.791 ± 0.349 for La IX and La X, respectively. However, given the limited number of interacting configurations introduced in the HFR calculations of Churilov & Joshi (2001) and Ryabtsev et al. (2002), which otherwise did not consider core-polarization effects (see Section 2), it is reasonable to assume that our HFR + CPOL results are more reliable than previously published data. The quality of our HFR + CPOL calculations could also be estimated in the particular case of $5s^2\ ^1S_0$–$5s5p\ ^{1,3}P_1$ transitions in La X for which Chou & Huang (1992), Curtis et al. (2000), and Biémont et al. (2000) calculated the radiative parameters. These data were found to be in good agreement with our results, the oscillator strengths obtained by Chou & Huang (1992) using the multiconfiguration relativistic random-phase approximation (MCRRPA) method being found to deviate by 10–25 per cent from our gf values, while the transition probabilities computed by Curtis et al. (2000) and Biémont et al. (2000) using the MCDHF approach show differences of 5–30 per cent compared to our gA values.

This is confirmed by the overall good agreement we found when comparing the radiative parameters obtained in our work using the HFR + CPOL, MCDHF, and AMBiT methods for the whole set of lanthanum ions of interest. Such comparisons are shown in Figs 3 and 4 in which our HFR + CPOL log gf values are plotted against MCDHF and AMBiT results, respectively. More precisely, we noted that the relative differences between HFR+CPOL and MCDHF oscillator strengths were in the range of 30–35 per cent for the majority of transitions in La V–X ions, whereas the mean deviations between HFR + CPOL and AMBiT gf values were found

Table 7. Transition probabilities (*gA*) and oscillator strengths (log *gf*) for experimentally observed lines in La IX.

λ_{obs} (Å)[a]	Transition		*gA* (s^{-1})		log *gf*
	Lower level	Upper level	Previous[b]	This work[c]	This work[c]
202.393	$5s^24f\ ^2F^o_{5/2}$	$5s^25g\ 593859_{7/2}$		2.63E + 11	0.19
202.824	$5s^24f\ ^2F^o_{7/2}$	$5s^25g\ 594699_{9/2}$		3.19E + 11	0.28
262.285	$5s^25p\ ^2P^o_{1/2}$	$5s^26s\ 381269.3_{1/2}$		4.05E + 10	− 0.39
283.280	$5s^25p\ ^2P^o_{3/2}$	$5s^26s\ 381269.3_{1/2}$		6.60E + 10	− 0.12
340.368	$5s^25p\ ^2P^o_{1/2}$	$5s5p4f\ 293802.3_{3/2}$		2.24E + 10	− 0.43
363.478	$5s5p^2\ 127670.4_{1/2}$	$4f5p^2\ 402790^o_{3/2}$	1.20E + 10	2.31E + 09	− 1.32
368.754	$5s^25p\ ^2P^o_{1/2}$	$5s5p4f\ 271182.1_{3/2}$		4.59E + 10	− 0.03
372.062	$5s^25p\ ^2P^o_{3/2}$	$5s5p4f\ 297037.6_{5/2}$		3.77E + 10	− 0.13
372.247	$5s5p^2\ 153628.1_{5/2}$	$5s5p5d\ 422273^o_{7/2}$	2.60E + 10	1.60E + 10	− 0.50
373.572	$5s5p^2\ 174459.3_{3/2}$	$5s5p5d\ 442148^o_{5/2}$	2.60E + 11	1.66E + 11	0.52
374.074	$5s5p^2\ 174459.3_{3/2}$	$5s^26p\ 441779^o_{1/2}$	7.00E + 09	4.75E + 09	− 1.03
375.118	$5s5p^2\ 191315.3_{1/2}$	$5s5p5d\ 457898^o_{1/2}$	3.00E + 10	3.31E + 10	− 0.18
377.367	$5s5p^2\ 184888.4_{5/2}$	$5s5p5d\ 449886^o_{7/2}$	2.24E + 11	6.08E + 10	0.11
377.367	$5s5p^2\ 143356.9_{3/2}$	$5s5p5d\ 408346^o_{3/2}$	8.10E + 10	2.55E + 10	− 0.26
377.717	$5s5p^2\ 143356.9_{3/2}$	$5s5p5d\ 408104^o_{5/2}$	7.80E + 10	5.34E + 10	0.04
378.157	$5s5p^2\ 143356.9_{3/2}$	$4f5p^2\ 407797^o_{1/2}$	4.20E + 10	1.19E + 10	− 0.61
382.215	$5s5p^2\ 143356.9_{3/2}$	$5s5p5d\ 404990^o_{1/2}$	2.40E + 10	4.77E + 10	0.01
382.303	$5s5p^2\ 143356.9_{3/2}$	$4f5p^2\ 404935^o_{3/2}$	6.00E + 09	3.86E + 09	− 1.09
384.691	$5s5p^2\ 127670.4_{1/2}$	$5s5p5d\ 387619^o_{1/2}$	9.20E + 10	7.78E + 10	0.23
385.951	$5s5p^2\ 127670.4_{1/2}$	$5s5p5d\ 386770^o_{3/2}$	1.12E + 11	1.02E + 11	0.35
391.946	$5s5p^2\ 153628.1_{5/2}$	$4f5p^2\ 408769^o_{7/2}$	3.20E + 10	8.17E + 09	− 0.75
392.590	$5s5p^2\ 153628.1_{5/2}$	$5s5p5d\ 408346^o_{3/2}$	3.20E + 10	1.96E + 10	− 0.34
392.960	$5s5p^2\ 153628.1_{5/2}$	$5s5p5d\ 408104^o_{5/2}$	1.24E + 11	9.45E + 10	0.32
393.098	$5s5p^2\ 153628.1_{5/2}$	$5s5p5d\ 408018^o_{7/2}$	2.34E + 11	1.92E + 11	0.63
394.802	$5s5p^2\ 184888.4_{5/2}$	$5s5p5d\ 438182^o_{7/2}$	1.06E + 11	6.08E + 10	0.11
395.074	$5s^25p\ ^2P^o_{1/2}$	$5s^25d\ 253117.3_{3/2}$		8.37E + 09	− 0.69
395.557	$5s5p4f\ 247782_{5/2}$	$5s^25f\ 500588^o_{7/2}$	2.90E + 10	1.18E + 10	− 0.60
399.607	$5s5p^2\ 191315.3_{1/2}$	$5s5p5d\ 441561^o_{1/2}$	2.80E + 10	3.31E + 10	− 0.18
399.867	$5s^25d\ 249703.5_{3/2}$	$5s^25f\ 499784^o_{5/2}$	1.02E + 11	1.14E + 11	0.41
400.478	$5s^25p\ ^2P^o_{1/2}$	$5s5p4f\ 249703.5_{3/2}$		4.59E + 10	0.03
400.599	$5s5p^2\ 143356.9_{3/2}$	$4f5p^2\ 392988^o_{3/2}$	7.00E + 09	5.10E + 09	− 0.93
402.380	$5s5p^2\ 143356.9_{3/2}$	$4f5p^2\ 391878^o_{5/2}$	2.60E + 10	1.58E + 10	− 0.44
402.961	$5s5p^2\ 127670.4_{1/2}$	$5p^3\ 375835^o_{3/2}$	7.00E + 09	7.54E + 09	− 0.75
404.216	$5s5p^2\ 153628.1_{5/2}$	$4f5p^2\ 401024^o_{5/2}$	2.20E + 10	3.51E + 10	− 0.08
405.407	$5s5p4f\ 253117.3_{3/2}$	$5s^25f\ 499784^o_{5/2}$	6.90E + 10	2.18E + 10	− 0.33
405.654	$5s5p4f\ 254070.0_{5/2}$	$5s^25f\ 500588^o_{7/2}$	1.02E + 11	2.42E + 11	0.78
406.546	$5s5p^2\ 174459.3_{3/2}$	$4f5p^2\ 420432^o_{5/2}$	1.50E + 10	9.99E + 08	− 1.60
406.819	$5s5p^2\ 191315.3_{1/2}$	$5s5p5d\ 437125^o_{3/2}$	1.13E + 11	7.89E + 10	0.29
409.397	$5s5p^2\ 143356.9_{3/2}$	$5s5p5d\ 387619^o_{1/2}$	2.00E + 09	1.63E + 09	− 1.40
410.820	$5s5p^2\ 143356.9_{3/2}$	$5s5p5d\ 386770^o_{3/2}$	2.50E + 10	2.21E + 10	− 0.27
411.272	$5s5p^2\ 221736.4_{3/2}$	$4f5p^2\ 464884^o_{5/2}$	1.31E + 11	2.48E + 09	− 1.19
411.363	$5s5p^2\ 153628.1_{5/2}$	$4f5p^2\ 396724^o_{7/2}$	4.10E + 10	5.55E + 10	0.13
411.670	$5s^25p\ ^2P^o_{3/2}$	$5s5p4f\ 271182.1_{3/2}$		1.15E + 10	− 0.55
412.502	$5s5p^2\ 174459.3_{3/2}$	$5s5p5d\ 416886^o_{3/2}$	5.20E + 10	4.54E + 10	0.04
413.257	$5s5p^2\ 221736.4_{3/2}$	$5s5p5d\ 463717^o_{3/2}$	1.21E + 11	1.55E + 07	− 3.40
414.094	$5s5p^2\ 221736.4_{3/2}$	$4f5p^2\ 463230^o_{5/2}$	1.40E + 11	1.88E + 11	0.67
415.112	$5s5p^2\ 143356.9_{3/2}$	$5s5p5d\ 384255^o_{5/2}$	1.06E + 11	1.07E + 11	0.42
415.599	$5s5p^2\ 153628.1_{5/2}$	$4f5p^2\ 394242^o_{5/2}$	8.00E + 09	9.44E + 09	− 0.63
421.169	$5s5p^2\ 220463.2_{1/2}$	$5s5p5d\ 457898^o_{1/2}$	2.80E + 10	3.16E + 10	− 0.02
421.247	$5s5p^2\ 184888.4_{5/2}$	$5s5p5d\ 422273^o_{7/2}$	3.50E + 10	5.60E + 10	0.15
422.810	$5s5p^2\ 191315.3_{1/2}$	$4f5p^2\ 427829^o_{3/2}$	1.90E + 10	7.89E + 10	0.29
422.987	$5s^25d\ 264176.5_{5/2}$	$5s^25f\ 500588^o_{7/2}$	2.36E + 11	2.42E + 11	0.78
423.890	$5s^25p\ ^2P^o_{3/2}$	$5s^25d\ 264176.5_{5/2}$		1.07E + 11	0.44
424.432	$5s^25d\ 264176.5_{5/2}$	$5s^25f\ 499784^o_{5/2}$	2.20E + 10	6.75E + 09	− 0.77
424.945	$5s5p^2\ 220463.2_{1/2}$	$5s5p5d\ 455788^o_{3/2}$	5.60E + 10	1.10E + 10	− 0.56
424.945	$5s5p^2\ 191315.3_{1/2}$	$4f5p^2\ 426634^o_{3/2}$	1.50E + 10	2.24E + 10	− 0.21
426.161	$5s5p^2\ 143356.9_{3/2}$	$4f5p^2\ 378012^o_{5/2}$	1.20E + 10	1.13E + 10	− 0.54
431.037	$5s5p^2\ 184888.4_{5/2}$	$5s5p5d\ 416886^o_{3/2}$	6.00E + 09	4.21E + 09	− 0.96

Table 7 – *continued*

λ_{obs} (Å)[a]	Transition		*gA* (s^{-1})		log *gf*
	Lower level	Upper level	Previous[b]	This work[c]	This work[c]
433.353	$5s5p^2\ 220463.2_{1/2}$	$5s^26p\ 451225^o_{3/2}$	4.60E + 10	4.51E + 09	– 0.91
433.602	$5s5p^2\ 153628.1_{5/2}$	$5s5p5d\ 384255^o_{5/2}$	2.30E + 10	1.78E + 10	– 0.32
435.102	$5s5p^2\ 184888.4_{5/2}$	$5s5p5d\ 414722^o_{5/2}$	1.11E + 11	8.35E + 10	0.35
435.742	$5s5p^2\ 221736.4_{3/2}$	$5s^26p\ 451225^o_{3/2}$	1.50E + 10	3.03E + 09	– 1.07
437.450	$5s5p4f\ 271182.1_{3/2}$	$5s^25f\ 499784^o_{5/2}$	8.70E + 10	9.61E + 10	0.40
442.862	$5s^25p\ ^2P^o_{3/2}$	$5s5p4f\ 254070.0_{5/2}$		2.75E + 10	– 0.10
444.737	$5s^25p\ ^2P^o_{3/2}$	$5s^25d\ 253117.3_{3/2}$		1.67E + 09	– 1.29
448.158	$5s5p^2\ 184888.4_{5/2}$	$5s5p5d\ 408018^o_{7/2}$	3.00E + 10	1.72E + 10	– 0.30
448.461	$5s5p^2\ 143356.9_{3/2}$	$5s5p5d\ 366348^o_{5/2}$	5.00E + 09	5.15E + 09	– 0.83
449.135	$5s^25p\ ^2P^o_{1/2}$	$5s5p4f\ 222651.2_{3/2}$		1.95E + 10	– 0.24
450.990	$5s^25p\ ^2P^o_{1/2}$	$5s5p^2\ 221736.4_{3/2}$		6.98E + 08	– 1.56
451.587	$5s^25p\ ^2P^o_{3/2}$	$5s5p4f\ 249703.5_{3/2}$		9.76E + 09	– 0.55
451.919	$5s5p^2\ 153628.1_{5/2}$	$5s5p5d\ 374907^o_{7/2}$	2.50E + 10	1.87E + 10	– 0.26
452.290	$5s5p^2\ 220463.2_{1/2}$	$5s5p5d\ 441561^o_{1/2}$	3.10E + 10	3.16E + 10	– 0.02
453.589	$5s^25p\ ^2P^o_{1/2}$	$5s5p^2\ 220463.2_{1/2}$		2.69E + 09	– 1.09
455.550	$5s^25p\ ^2P^o_{3/2}$	$5s5p4f\ 247782^o_{5/2}$	1.10E + 09	4.67E + 09	– 0.84
457.602	$5s5p^2\ 174459.3_{3/2}$	$4f5p^2\ 392988^o_{3/2}$	2.80E + 10	2.65E + 10	– 0.10
457.970	$5s5p^2\ 143356.9_{3/2}$	$5s5p5d\ 361709^o_{3/2}$	2.00E + 09	2.13E + 09	– 1.19
459.950	$5s5p^2\ 174459.3_{3/2}$	$4f5p^2\ 391878^o_{5/2}$	2.90E + 10	4.72E + 09	– 0.79
465.562	$5s5p^2\ 221736.4_{3/2}$	$4f5p^2\ 436530^o_{5/2}$	1.40E + 10	6.62E + 09	– 0.67
470.099	$5s5p^2\ 153628.1_{5/2}$	$5s5p5d\ 366348^o_{5/2}$	8.00E + 09	5.15E + 09	– 0.83
471.012	$5s5p^2\ 174459.3_{3/2}$	$5s5p5d\ 386770^o_{3/2}$	1.20E + 10	5.44E + 09	– 0.75
483.863	$5s5p^2\ 127670.4_{1/2}$	$5p^3\ 334342^o_{3/2}$	1.00E + 10	1.06E + 10	– 0.45
495.856	$5s5p^2\ 191315.3_{1/2}$	$4f5p^2\ 392988^o_{3/2}$	1.60E + 10	1.24E + 10	– 0.33
498.255	$5s5p4f\ 225404.0_{9/2}$	$4f5p^2\ 426108^o_{11/2}$	2.60E + 10	2.34E + 10	– 0.07
510.805	$5s5p4f\ 234301.4_{7/2}$	$4f5p^2\ 430074^o_{9/2}$	2.30E + 10	1.74E + 10	– 0.17
511.832	$5s^24f\ ^2F^o_{7/2}$	$5s5p4f\ 297037.6_{5/2}$		1.01E + 11	0.59
513.434	$5s5p4f\ 231868.2_{5/2}$	$4f5p^2\ 426634^o_{3/2}$	2.30E + 10	4.62E + 09	– 0.75
514.440	$5s^25p\ ^2P^o_{3/2}$	$5s5p4f\ 222651.2_{3/2}$		6.85E + 10	0.41
515.377	$5s^24f\ ^2P^o_{5/2}$	$5s5p4f\ 293802.3_{3/2}$		7.00E + 10	0.44
516.870	$5s^25p\ ^2P^o_{3/2}$	$5s5p^2\ 221736.4_{3/2}$		2.90E + 08	– 2.05
519.629	$5s^25d\ 249703.5_{3/2}$	$5s5p5d\ 442148^o_{5/2}$	2.30E + 10	1.51E + 10	– 0.22
520.300	$5s^25p\ ^2P^o_{3/2}$	$5s5p^2\ 220463.2_{1/2}$		2.26E + 10	– 0.06
520.629	$5s^25d\ 249703.5_{3/2}$	$5s^26p\ 441779^o_{1/2}$	5.00E + 09	2.29E + 09	– 1.05
521.889	$5s^25d\ 264176.2_{5/2}$	$5s5p5d\ 455788^o_{3/2}$	3.10E + 10	1.83E + 10	– 0.16
522.697	$5s^25p\ ^2P^o_{1/2}$	$5s5p^2\ 191315.3_{1/2}$		3.03E + 10	0.07
523.601	$5s5p^2\ 143356.9_{3/2}$	$5p^3\ 334342^o_{3/2}$	1.30E + 10	2.13E + 10	– 0.09
523.703	$5s5p^2\ 184888.4_{5/2}$	$5p^3\ 375835^o_{3/2}$	2.40E + 10	1.81E + 10	– 0.15
527.468	$5s5p^2\ 127670.4_{1/2}$	$5p^3\ 317255^o_{3/2}$	1.20E + 10	1.06E + 10	– 0.45
528.240	$5s5p4f\ 260578_{9/2}$	$5s5p5d\ 449886^o_{7/2}$	6.10E + 10	3.88E + 09	– 0.75
531.949	$5s5p4f\ 216947.8_{5/2}$	$4f5p^2\ 404935^o_{3/2}$	2.60E + 10	2.30E + 10	– 0.01
534.050	$5s5p^2\ 174459.3_{3/2}$	$5s5p5d\ 361709^o_{3/2}$	3.00E + 09	1.58E + 09	– 1.18
536.731	$5s5p^2\ 174459.3_{3/2}$	$5p^3\ 360769^o_{1/2}$	2.10E + 10	1.40E + 10	– 0.24
537.262	$5s5p4f\ 234301.4_{7/2}$	$4f5p^2\ 420432^o_{5/2}$	2.90E + 10	2.42E + 10	0.01
538.134	$5s5p4f\ 279688.7_{7/2}$	$4f5p^2\ 465514^o_{7/2}$	5.20E + 10	2.75E + 10	0.09
541.283	$5s5p4f\ 251778_{7/2}$	$4f5p^2\ 436530^o_{5/2}$	3.00E + 10	3.30E + 10	0.14
541.605	$5s^24f\ ^2F^o_{5/2}$	$5s5p4f\ 284406.6_{7/2}$		6.26E + 10	0.47
544.876	$5s5p4f\ 219995.4_{7/2}$	$4f5p^2\ 403523^o_{5/2}$	2.10E + 10	1.52E + 10	– 0.18
545.227	$5s^24f\ ^2F^o_{7/2}$	$5s5p4f\ 285070.3_{9/2}$		1.13E + 11	0.70
546.190	$5s5p4f\ 244249_{9/2}$	$4f5p^2\ 427335^o_{9/2}$	4.20E + 10	3.30E + 10	0.16
546.355	$5s5p4f\ 244249_{9/2}$	$4f5p^2\ 427277^o_{7/2}$	3.50E + 10	2.91E + 10	0.10
546.449	$5s5p^2\ 153628.1_{5/2}$	$5p^3\ 336627^o_{5/2}$	7.00E + 09	2.64E + 09	– 0.94
547.212	$5s^24f\ ^2F^o_{7/2}$	$5s5p4f\ 284406.6_{7/2}$		9.50E + 09	– 0.37
547.450	$5s5p4f\ 224528.1_{7/2}$	$4f5p^2\ 407192^o_{9/2}$	1.30E + 10	1.09E + 10	– 0.32
548.998	$5s5p4f\ 219995.4_{7/2}$	$4f5p^2\ 402146^o_{9/2}$	3.20E + 10	3.23E + 10	0.16
550.021	$5s5p4f\ 245526.8_{7/2}$	$4f5p^2\ 427335^o_{9/2}$	1.90E + 10	1.79E + 10	– 0.11
550.214	$5s5p4f\ 245526.8_{7/2}$	$4f5p^2\ 427277^o_{7/2}$	2.30E + 10	1.39E + 10	– 0.21
550.528	$5s5p4f\ 245526.8_{7/2}$	$4f5p^2\ 427173^o_{5/2}$	2.60E + 10	1.87E + 10	– 0.08

Table 7 – *continued*

λ_{obs} (Å)[a]	Transition		gA (s^{-1})		log gf
	Lower level	Upper level	Previous[b]	This work[c]	This work[c]
552.400	5s5p4f $219995.4_{7/2}$	4f5p^2 $401024^o_{5/2}$	1.40E + 10	8.27E + 09	− 0.42
553.360	5s5p^2 $153628.1_{5/2}$	5p^3 $334342^o_{3/2}$	1.60E + 10	1.91E + 10	− 0.09
553.794	5s5p4f $246760.0_{11/2}$	4f5p^2 $427335^o_{9/2}$	4.30E + 10	3.34E + 10	0.18
554.192	5s5p4f $285070.3_{9/2}$	4f5p^2 $465514^o_{7/2}$	8.30E + 10	4.49E + 10	0.33
555.810	5s^{2}4f ^{2}F$^o_{5/2}$	5s5p4f $279688.7_{7/2}$		1.01E + 10	− 0.33
557.119	5s5p4f $247782_{5/2}$	4f5p^2 $427277^o_{7/2}$	2.00E + 10	4.85E + 09	− 0.66
557.579	5s5p4f $246760_{11/2}$	4f5p^2 $426108^o_{11/2}$	5.60E + 10	4.37E + 10	0.30
559.208	5s5p4f $284406.6_{7/2}$	4f5p^2 $463230^o_{5/2}$	3.00E + 10	1.77E + 08	− 2.10
560.309	5s^{2}4f ^{2}F$^o_{5/2}$	5s5p4f $278244.0_{5/2}$		6.26E + 10	0.47
561.708	5s^{2}5p ^{2}F$^o_{7/2}$	5s5p4f $279688.7_{7/2}$		7.81E + 10	0.56
563.001	5s5p4f $224528.1_{7/2}$	4f5p^2 $402146^o_{9/2}$	2.30E + 10	9.17E + 09	− 0.37
563.613	5s5p4f $225404.0_{9/2}$	4f5p^2 $402830^o_{7/2}$	2.20E + 10	1.17E + 10	− 0.26
563.847	5s5p4f $219995.4_{7/2}$	4f5p^2 $397350^o_{9/2}$	2.30E + 10	3.23E + 10	0.16
564.224	5s5p4f $225404.0_{9/2}$	4f5p^2 $402638^o_{11/2}$	4.80E + 10	3.44E + 10	0.20
565.288	5s5p4f $231868.2_{5/2}$	4f5p^2 $408769^o_{7/2}$	3.20E + 10	2.06E + 10	− 0.02
565.483	5s5p4f $224184.0_{5/2}$	4f5p^2 $401024^o_{5/2}$	9.00E + 09	5.32E + 09	− 0.59
565.820	5s5p4f $219995.4_{7/2}$	4f5p^2 $396724^o_{7/2}$	1.60E + 10	9.74E + 09	− 0.33
568.073	5s5p4f $216947.8_{5/2}$	4f5p^2 $392986^o_{7/2}$	1.20E + 10	7.03E + 09	− 0.47
571.660	5s5p4f $216947.8_{5/2}$	4f5p^2 $391878^o_{5/2}$	1.10E + 10	8.89E + 09	− 0.37
573.200	5s^{2}5p ^{2}P$^o_{1/2}$	5s5p^2 $174459.3_{3/2}$		9.93E + 09	− 0.30
574.516	5s5p4f $253117.3_{3/2}$	4f5p^2 $427173^o_{5/2}$	1.60E + 10	1.35E + 10	− 0.20
574.688	5s^{2}5d $264176.5_{5/2}$	5s5p5d $438182^o_{7/2}$	1.00E + 10	3.31E + 10	0.20
575.044	5s5p^2 $143356.9_{3/2}$	5p^3 $317255^o_{3/2}$	1.00E + 10	2.13E + 10	− 0.09
575.529	5s5p4f $252879_{1/2}$	4f5p^2 $426634^o_{3/2}$	8.00E + 09	8.74E + 09	− 0.38
577.353	5s5p4f $254070.0_{5/2}$	4f5p^2 $427277^o_{7/2}$	1.00E + 10	5.26E + 09	− 0.59
578.399	5s5p4f $234301.4_{7/2}$	4f5p^2 $407192^o_{9/2}$	1.10E + 10	4.74E + 09	− 0.63
579.571	5s5p4f $224184.0_{5/2}$	4f5p^2 $396724^o_{7/2}$	2.10E + 10	1.19E + 10	− 0.23
580.196	5s^{2}5d $264176.5_{5/2}$	4f5p^2 $436530^o_{5/2}$	1.20E + 10	4.81E + 09	− 0.62
581.571	5s5p4f $225404.0_{9/2}$	4f5p^2 $397350^o_{9/2}$	9.00E + 09	6.85E + 09	− 0.49
582.786	5s5p4f $222651.2_{3/2}$	4f5p^2 $394242^o_{5/2}$	1.00E + 10	4.87E + 09	− 0.62
586.182	5s5p4f $271182.1_{3/2}$	5s^{2}6p $441779^o_{1/2}$	3.00E + 09	8.92E + 08	− 1.37
589.979	5s5p4f $260578_{9/2}$	4f5p^2 $430074^o_{9/2}$	5.20E + 10	4.19E + 10	0.33
590.128	5s5p^2 $191315.3_{1/2}$	5p^3 $360769^o_{1/2}$	2.00E + 09	5.56E + 08	− 1.53
590.920	5s5p4f $222651.2_{3/2}$	4f5p^2 $391878^o_{5/2}$	5.00E + 09	5.15E + 09	− 0.58
593.610	5s5p4f $224528.1_{7/2}$	4f5p^2 $392986^o_{7/2}$	6.00E + 09	5.09E + 09	− 0.57
603.487	5s5p4f $224528.1_{7/2}$	5s5p5d $390232^o_{9/2}$	4.00E + 09	1.27E + 09	− 1.15
604.784	5s5p4f $271182.1_{3/2}$	4f5p^2 $436529^o_{5/2}$	2.20E + 10	9.79E + 09	− 0.28
611.150	5s5p^2 $153628.1_{5/2}$	5p^3 $317255^o_{3/2}$	2.40E + 10	1.91E + 10	− 0.09
613.313	5s^{2}5p ^{2}P$^o_{3/2}$	5s5p^2 $191315.3_{1/2}$		8.57E + 08	− 1.35
613.704	5s5p4f $251778_{7/2}$	5s5p5d $414722^o_{5/2}$	5.00E + 09	2.38E + 09	− 0.89
614.188	5s5p4f $254070.0_{5/2}$	5s5p5d $416886^o_{3/2}$	6.00E + 09	2.88E + 09	− 0.81
615.100	5s5p4f $245526.8_{7/2}$	5s5p5d $408104^o_{5/2}$	1.10E + 10	1.09E + 10	− 0.21
622.460	5s5p4f $224184.0_{5/2}$	4f5p^2 $384837^o_{7/2}$	8.00E + 09	1.19E + 10	− 0.23
622.806	5s5p4f $247782_{5/2}$	5s5p5d $408346^o_{3/2}$	7.00E + 09	1.72E + 08	− 1.98
623.797	5s5p4f $224528.1_{7/2}$	4f5p^2 $384837^o_{7/2}$	1.20E + 10	1.14E + 08	− 2.24
627.224	5s5p4f $225404.0_{9/2}$	4f5p^2 $384837^o_{7/2}$	4.00E + 10	1.19E + 08	− 2.22
632.843	5s5p4f $219995.4_{7/2}$	4f5p^2 $378012^o_{5/2}$	1.20E + 10	7.46E + 09	− 0.36
638.478	5s^{2}5p ^{2}P$^o_{3/2}$	5s5p^2 $184888.4_{5/2}$		6.27E + 09	− 0.40
641.531	5s5p4f $246760_{11/2}$	4f5p^2 $402638^o_{11/2}$	4.40E + 10	3.15E + 10	0.27
643.560	5s5p4f $246760_{11/2}$	4f5p^2 $402146^o_{9/2}$	3.70E + 10	2.75E + 10	0.22
648.938	5s5p^2 $221736.4_{3/2}$	5p^3 $375835^o_{3/2}$	1.30E + 10	5.49E + 09	− 0.44
653.167	5s5p4f $244249_{9/2}$	4f5p^2 $397350^o_{9/2}$	2.30E + 10	7.46E + 09	− 0.36
655.850	5s5p4f $244249_{9/2}$	4f5p^2 $396724^o_{7/2}$	1.40E + 10	7.32E + 09	− 0.34
657.646	5s5p4f $252879_{1/2}$	4f5p^2 $404935^o_{3/2}$	9.00E + 09	5.27E + 09	− 0.48
657.864	5s^{2}4f ^{2}F$^o_{5/2}$	5s5p4f $251778_{7/2}$	1.00E + 09	3.86E + 08	− 1.57
659.030	5s5p^2 $184888.4_{5/2}$	5p^3 $336627^o_{5/2}$	1.60E + 10	1.04E + 09	− 1.10
662.033	5s5p4f $251778_{7/2}$	4f5p^2 $402830^o_{7/2}$	8.00E + 09	3.61E + 08	− 1.61
664.290	5s5p4f $234301.4_{7/2}$	4f5p^2 $384837^o_{7/2}$	2.00E + 10	1.95E + 09	− 0.96

Table 7 – *continued*

λ_{obs} (Å)[a]	Transition		gA (s^{-1})		log gf
	Lower level	Upper level	Previous[b]	This work[c]	This work[c]
666.144	$5s^24f\ ^2F^o_{7/2}$	$5s5p4f\ 251778_{7/2}$	2.00E + 09	7.01E + 08	− 1.29
674.798	$5s5p4f\ 260578_{9/2}$	$4f5p^2\ 408769^o_{7/2}$	1.10E + 10	7.44E + 09	− 0.31
675.626	$5s^24f\ ^2F^o_{5/2}$	$5s5p4f\ 247782_{5/2}$	7.00E + 09	2.82E + 08	− 1.68
678.145	$5s5p4f\ 245526.8_{7/2}$	$4f5p^2\ 392986^o_{7/2}$	1.20E + 10	6.98E + 09	− 0.33
682.068	$5s5p4f\ 260578_{9/2}$	$4f5p^2\ 407192^o_{9/2}$	1.50E + 10	1.14E + 10	− 0.12
684.024	$5s^25p\ ^2P^o_{3/2}$	$5s5p^2\ 174459.3_{3/2}$		1.06E + 08	− 2.13
690.791	$5s5p4f\ 216947.8_{5/2}$	$5s5p5d\ 361709^o_{3/2}$	3.00E + 09	2.98E + 09	− 0.66
695.090	$5s^24f\ ^2F^o_{7/2}$	$5s5p4f\ 245526.8_{7/2}$		7.39E + 08	− 1.23
696.996	$5s5p4f\ 246760_{11/2}$	$5s5p5d\ 390232^o_{9/2}$	2.00E + 09	5.07E + 09	− 0.42
700.298	$5s5p^2\ 174459.3_{3/2}$	$5p^3\ 317255^o_{3/2}$	4.00E + 09	1.11E + 09	− 1.21
709.024	$5s5p4f\ 285070.3_{9/2}$	$4f5p^2\ 426108^o_{11/2}$	1.90E + 10	1.19E + 10	− 0.02
711.208	$5s5p4f\ 234301.4_{7/2}$	$5s5p5d\ 374907^o_{7/2}$	3.00E + 09	2.13E + 09	− 0.78
712.734	$5s5p^2\ 220463.2_{1/2}$	$5p^3\ 360769^o_{1/2}$	6.00E + 09	2.99E + 09	− 0.64
743.330	$5s^24f\ ^2F^o_{5/2}$	$5s5p4f\ 234301.4_{7/2}$		1.64E + 08	− 1.83
753.911	$5s^24f\ ^2F^o_{7/2}$	$5s5p4f\ 234301.4_{7/2}$		8.95E + 08	− 1.08
757.023	$5s^24f\ ^2F^o_{5/2}$	$5s5p4f\ 231868.2_{5/2}$		1.96E + 08	− 1.74
768.001	$5s^24f\ ^2F^o_{7/2}$	$5s5p4f\ 231868.2_{5/2}$		4.98E + 08	− 1.32
783.265	$5s^25p\ ^2P^o_{1/2}$	$5s5p^2\ 127670.4_{1/2}$		2.95E + 08	− 1.55
794.035	$5s5p^2\ 191315.3_{1/2}$	$5p^3\ 317255^o_{3/2}$	3.00E + 09	8.19E + 08	− 1.20
797.689	$5s^25p\ ^2P^o_{3/2}$	$5s5p^2\ 153628.1_{5/2}$		9.16E + 08	− 1.04
801.563	$5s^24f\ ^2F^o_{5/2}$	$5s5p4f\ 224528.1_{7/2}$		7.78E + 08	− 1.09
803.775	$5s^24f\ ^2F^o_{5/2}$	$5s5p4f\ 224184.0_{5/2}$		5.18E + 08	− 1.26
808.124	$5s^24f\ ^2F^o_{7/2}$	$5s5p4f\ 225404.0_{9/2}$		8.49E + 08	− 1.04
813.880	$5s^24f\ ^2F^o_{7/2}$	$5s5p4f\ 224528.1_{7/2}$		4.59E + 08	− 1.30
831.779	$5s^24f\ ^2F^o_{5/2}$	$5s5p4f\ 219995.4_{7/2}$		1.80E + 08	− 1.70
853.412	$5s^24f\ ^2F^o_{5/2}$	$5s5p4f\ 216947.8_{5/2}$		9.14E + 07	− 1.97
868.878	$5s^25p\ ^2P^o_{3/2}$	$5s5p^2\ 143356.9_{3/2}$		8.37E + 07	− 2.00
870.394	$5s5p^2\ 221736.4_{3/2}$	$5p^3\ 336627^o_{5/2}$	4.00E + 09	2.35E + 09	− 0.52
1006.004	$5s^25p\ ^2P^o_{3/2}$	$5s5p^2\ 127670.4_{1/2}$		2.70E + 07	− 2.37

[a]Gayasov & Joshi (1998) and Churilov & Joshi (2001); [b]Churilov & Joshi (2001); [c]HFR + CPOL calculations.

to be around 30 per cent in the case of La V, La VIII, and La X ions. Looking in more detail at Figs 3 and 4, however, we notice some larger discrepancies between the different theoretical methods. These concern a rather small number of specific cases for which the line strength calculations were found to be affected by severe cancellation effects. This is for example the case of the three points that deviate strongly from the diagonal in Fig. 4. These correspond to the transitions at $\lambda = 370.024$, 411.267 (La VIII), and 564.420 Å (La X) for which the cancellation factor (CF), as defined by Cowan (1981), reached the very small values of 0.003, 0.007, and 0.006, respectively, in our HFR + CPOL calculations, indicating that the corresponding oscillator strengths were probably underestimated and to be taken with care. Nevertheless, these few punctual problems do not alter the opacity calculations that rely on the global accuracy of the atomic data used.

Following these considerations, we can conclude that the radiative data calculated in our work using the HFR + CPOL approach constitute a sufficiently reliable basis, in quantity and quality, for the estimation of opacities due to La V–X ions in kilonovae.

5 OPACITY CALCULATIONS

For the calculations of opacities, we used exactly the same procedure as the one employed in our previous study focused on Ce V–X ions (Carvajal Gallego et al. 2022). As a reminder, the bound–bound opacity is calculated using the following formula (see e.g. Karp et al. 1977; Eastman & Pinto 1993; Kasen, Thomas & Nugent 2006):

$$\kappa^{\rm bb}(\lambda) = \frac{1}{\rho c t} \sum_l \frac{\lambda_l}{\Delta\lambda}(1 - {\rm e}^{-\tau_l}), \tag{2}$$

where λ (in Å) is the central wavelength within the region of width $\Delta\lambda$, λ_l are the wavelengths of the lines appearing in this range, τ_l are the corresponding optical depths, c (in cm s^{-1}) is the speed of light, ρ (in g cm^{-3}) is the density of the ejected gas, and t (in s) is the elapsed time since ejection.

The optical depth can be expressed using the Sobolev (1960) expression:

$$\tau_l = \frac{\pi e^2}{m_{\rm e} c} f_l n_l t \lambda_l, \tag{3}$$

where e (in C) is the elementary charge, $m_{\rm e}$ (in g) is the electron mass, f_l (dimensionless) is the oscillator strength, and n_l (in cm^{-3}) is the density of the lower level of the transition.

Since the local thermodynamic equilibrium (LTE) is assumed in this formalism, n_l can be expressed using the Boltzmann distribution:

$$n_l = \frac{g_l}{g_0} n\, {\rm e}^{-E_l/k_{\rm B}T}, \tag{4}$$

where $k_{\rm B}$ is the Boltzmann constant (in cm^{-1} K^{-1}), T (in K) is the temperature, g_l and E_l (in cm^{-1}) are, respectively, the statistical weight and the energy of the lower level of the transition, and g_0 is the statistical weight of the ground level for the ion considered.

Table 8. Transition probabilities (gA) and oscillator strengths (log gf) for experimentally observed lines in La X.

λ_{obs} (Å)[a]	Transition		gA (s^{-1})		log gf
	Lower level	Upper level	Previous[a]	This work[b]	This work[b]
160.066	$5s^2\ ^1S_0$	$5s6p\ ^1P^o_1$	3.47E + 10	3.27E + 10	− 0.90
162.335	$5s^2\ ^1S_0$	$5s6p\ ^3P^o_1$	1.17E + 10	9.95E + 09	− 1.40
236.951	$5s5p\ ^3P^o_0$	$5s6s\ ^3S_1$	2.08E + 10	2.44E + 10	− 0.68
240.719	$5s5p\ ^3P^o_1$	$5s6s\ ^3S_1$	5.57E + 10	6.66E + 10	− 0.24
255.507	$5s5p\ ^3P^o_2$	$5s6s\ ^3S_1$	8.28E + 10	9.84E + 10	− 0.02
272.757	$5s5p\ ^1P^o_1$	$5s6s\ ^1S_0$	4.00E + 10	4.35E + 10	− 0.30
280.140	$5s5p\ ^1P^o_1$	$5s6s\ ^3S_1$	2.40E + 09	1.90E + 09	− 1.63
335.339	$5p^2\ ^3P_1$	$4f5d\ ^3D^o_2$	1.30E + 10	1.02E + 10	− 0.75
335.638	$5s5p\ ^3P^o_1$	$5s5d\ ^1D_2$	9.80E + 09	3.13E + 09	− 1.29
337.243	$5p^2\ ^1D_2$	$4f5d\ ^3D^o_3$	3.48E + 10	2.70E + 10	− 0.33
363.174	$5p^2\ ^1D_2$	$5p5d\ ^1F^o_3$	5.74E + 10	5.76E + 10	0.06
366.409	$5s5p\ ^3P^o_0$	$5s5d\ ^3D_1$	5.09E + 10	3.95E + 10	− 0.11
369.473	$5p^2\ ^3P_2$	$5s6p\ ^3P^o_1$	6.50E + 09	4.31E + 09	− 1.09
374.335	$5s5p\ ^3P^o_1$	$5s5d\ ^3D_2$	1.17E + 11	9.19E + 10	0.28
374.675	$5p^2\ ^3P_1$	$5p5d\ ^3P^o_1$	6.89E + 10	5.30E + 10	0.06
375.498	$5s5p\ ^3P^o_1$	$5s5d\ ^3D_1$	3.33E + 10	3.31E + 09	− 1.29
376.079	$4f5p\ ^3G_4$	$4f5d\ ^1H^o_5$	3.88E + 10	3.50E + 10	− 0.12
380.193	$5p^2\ ^3P_0$	$5p5d\ ^3D^o_1$	1.23E + 11	9.12E + 10	0.31
383.615	$5p^2\ ^1D_2$	$5p5d\ ^3D^o_3$	1.92E + 11	1.57E + 11	0.54
383.615	$4f5p\ ^3F_3$	$4f5d\ ^3D^o_3$	3.62E + 10	3.84E + 10	− 0.05
384.314	$4f5p\ ^3F_3$	$4f5d\ ^3D^o_2$	8.63E + 10	7.01E + 10	0.20
386.512	$4f5p\ ^3G_4$	$4f5d\ ^3D^o_3$	3.56E + 10	3.24E + 10	− 0.13
388.989	$5s5p\ ^3P^o_0$	$4f5p\ ^3D_1$	1.11E + 10	3.95E + 10	− 0.11
390.180	$5p^2\ ^3P_1$	$5p5d\ ^3D^o_2$	1.10E + 11	8.17E + 10	0.28
393.523	$5p^2\ ^1D_2$	$5p5d\ ^3D^o_2$	4.86E + 10	2.80E + 10	− 0.18
393.698	$4f5p\ ^3G_3$	$4f5d\ ^3H^o_4$	8.11E + 10	6.67E + 10	0.20
394.309	$4f5p\ ^3G_3$	$4f5d\ ^3F^o_3$	2.71E + 10	2.38E + 10	− 0.24
395.986	$5s5d\ ^3D_1$	$5s5f\ ^3F^o_2$	1.64E + 11	1.23E + 11	0.46
396.578	$5s5d\ ^3D_2$	$5s5f\ ^3F^o_3$	2.63E + 11	1.99E + 11	0.67
396.865	$4f5p\ ^3G_3$	$4f5d\ ^3F^o_2$	2.94E + 10	2.38E + 10	− 0.24
398.083	$4f5p\ ^3G_4$	$4f5d\ ^3G^o_4$	4.01E + 10	4.53E + 09	− 0.96
398.865	$4f5p\ ^3G_4$	$4f5d\ ^3H^o_5$	2.11E + 11	5.21E + 10	0.11
399.220	$4f5p\ ^3G_3$	$4f5d\ ^1G^o_4$	1.51E + 11	1.16E + 11	0.45
399.250	$5s5p\ ^3P^o_1$	$4f5p\ ^3D_1$	7.20E + 09	7.82E + 09	− 0.73
399.397	$5s5d\ ^3D_3$	$5s5f\ ^3F^o_4$	4.08E + 11	3.20E + 11	0.88
399.622	$4f5p\ ^3F_3$	$4f5d\ ^3H^o_4$	6.57E + 10	4.44E + 10	0.04
400.254	$4f5p\ ^3F_3$	$4f5d\ ^3F^o_3$	9.40E + 10	2.37E + 10	− 0.23
401.941	$4f5p\ ^3F_2$	$4f5d\ ^3F^o_2$	9.51E + 10	7.66E + 10	0.28
402.758	$4f5p\ ^3G_4$	$4f5d\ ^3H^o_4$	7.46E + 10	5.21E + 10	0.11
404.193	$5p^2\ ^3P_2$	$5p5d\ ^1F^o_3$	1.52E + 11	1.23E + 11	0.48
404.193	$5s5p\ ^3P^o_1$	$4f5p\ ^3D_2$	1.20E + 10	1.11E + 10	− 0.57
405.283	$4f5p\ ^3F_3$	$4f5d\ ^1G^o_4$	2.42E + 10	1.92E + 10	− 0.31
407.301	$5s5p\ ^3P^o_2$	$5s5d\ ^3D_3$	1.20E + 10	1.48E + 11	0.55
408.517	$4f5p\ ^3G_4$	$4f5d\ ^1G^o_4$	3.18E + 10	2.23E + 10	− 0.24
411.346	$5s5p\ ^3P^o_2$	$5s5d\ ^3D_2$	3.04E + 10	2.41E + 10	− 0.23
417.550	$5s5p\ ^1P^o_1$	$5s5d\ ^1D_2$	1.53E + 11	6.57E + 10	0.24
420.342	$5p^2\ ^3P_2$	$5p5d\ ^3P^o_2$	1.18E + 11	8.33E + 10	0.35
421.312	$4f5p\ ^1F_3$	$4f5d\ ^3D^o_3$	2.98E + 10	2.66E + 10	− 0.12
422.185	$4f5p\ ^1F_3$	$4f5d\ ^3D^o_2$	1.61E + 10	3.19E + 09	− 1.04
422.704	$5p^2\ ^3P_1$	$5p5d\ ^1D^o_2$	7.97E + 10	4.91E + 10	0.13
422.969	$4f5p\ ^3D_3$	$4f5d\ ^3P^o_2$	6.93E + 10	5.67E + 10	0.19
424.142	$5s5d\ ^1D_2$	$5s5f\ ^1F^o_3$	3.10E + 11	1.26E + 11	0.54
426.173	$4f5p\ ^3F_4$	$4f5d\ ^3D^o_3$	2.73E + 10	2.44E + 10	− 0.17
426.610	$5p^2\ ^1D_2$	$5p5d\ ^1D^o_2$	4.30E + 10	3.85E + 10	0.03
429.695	$5p^2\ ^3P_2$	$5p5d\ ^3D^o_3$	7.31E + 10	6.11E + 10	0.23
432.371	$4f5p\ ^3D_3$	$4f5d\ ^3D^o_3$	2.98E + 10	2.66E + 10	− 0.12
432.647	$4f5p\ ^1F_3$	$4f5d\ ^3P^o_4$	6.23E + 10	1.82E + 10	− 0.27
433.343	$4f5p\ ^1G_4$	$4f5d\ ^1H^o_5$	2.41E + 11	1.88E + 11	0.73
434.237	$4f5p\ ^3F_4$	$4f5d\ ^3G^o_5$	1.79E + 11	1.31E + 11	0.58
435.104	$4f5p\ ^1F_3$	$4f5d\ ^3G^o_4$	6.72E + 10	3.35E + 10	− 0.02
435.386	$5p^2\ ^1D_2$	$5p5d\ ^3F^o_3$	3.32E + 10	1.74E + 10	− 0.29
437.515	$5p^2\ ^1S_0$	$4f5d\ ^1P^o_1$	5.75E + 10	7.20E + 07	− 2.72

Table 8 – *continued*

λ_{obs} (Å)[a]	Transition		gA (s^{-1})		log gf
	Lower level	Upper level	Previous[a]	This work[b]	This work[b]
437.765	4f5p $^3F_4$	4f5d $^3F^o_4$	6.33E + 10	1.82E + 10	− 0.27
440.709	4f5p $^1F_3$	4f5d $^3H^o_4$	4.74E + 10	4.84E + 10	0.15
441.273	4f5p $^3F_4$	4f5d $^3H^o_5$	6.04E + 10	5.79E + 10	0.23
441.561	4f5p $^3G_5$	4f5d $^3H^o_6$	3.12E + 11	2.49E + 11	0.87
441.845	4f5p $^3G_5$	4f5d $^3G^o_5$	7.23E + 10	6.11E + 10	0.26
444.310	4f5p $^3D_3$	4f5d $^3F^o_4$	6.69E + 10	1.18E + 10	− 0.44
445.263	5s5p $^3P^o_2$	4f5p $^3D_3$	1.00E + 10	1.26E + 10	− 0.44
447.604	4f5p $^1F_3$	4f5d $^1G^o_4$	5.40E + 09	6.32E + 09	− 0.72
449.110	4f5p $^3G_5$	4f5d $^3H^o_5$	2.98E + 10	2.08E + 10	− 0.19
453.110	4f5p $^3F_4$	4f5d $^1G^o_4$	7.80E + 09	6.24E + 09	− 0.71
457.348	5s5p $^3P^o_1$	4f5p $^3F_2$	1.30E + 09	9.66E + 08	− 1.53
458.894	5s5d $^3D_2$	4f5d $^3P^o_2$	1.51E + 10	1.44E + 10	− 0.33
460.645	5p^2 $^1D_2$	5p5d $^3F^o_2$	1.84E + 10	1.06E + 10	− 0.46
462.509	4f5s $^1F^o_3$	5s5d $^1D_2$	3.69E + 10	2.04E + 10	− 0.19
462.806	4f5p $^1G_4$	4f5d $^3G^o_4$	3.98E + 10	2.21E + 07	− 3.15
463.658	5s5d $^3D_1$	5s6p $^3P^o_1$	1.91E + 10	1.44E + 10	− 0.32
463.871	4f5p $^1G_4$	4f5d $^3H^o_5$	1.48E + 10	1.43E + 10	− 0.33
464.043	5s5d $^3D_3$	4f5d $^3P^o_2$	1.84E + 10	1.94E + 10	− 0.20
465.442	5s5d $^3D_2$	5s6p $^3P^o_1$	3.04E + 10	2.54E + 10	− 0.07
473.164	5s5p $^3P^o_1$	5p^2 $^3P_2$	1.21E + 10	1.07E + 10	− 0.45
476.986	4f5p $^1G_4$	4f5d $^1G^o_4$	3.83E + 10	3.60E + 10	0.10
489.580	4f5p $^1D_2$	4f5d $^1F^o_3$	1.58E + 10	2.49E + 10	− 0.13
510.164	5s5p $^1P^o_1$	4f5p $^1D_2$	1.83E + 10	1.26E + 10	− 0.29
511.328	4f5s $^3F^o_3$	5s5d $^3D_3$	5.50E + 09	5.74E + 09	− 0.64
514.661	4f5s $^3F^o_4$	5s5d $^3D_3$	4.03E + 10	4.28E + 10	0.24
515.852	4f5s $^3F^o_2$	5s5d $^3D_2$	6.40E + 09	6.63E + 09	− 0.57
517.743	4f5s $^3F^o_3$	5s5d $^3D_2$	3.19E + 10	3.38E + 10	0.14
518.068	4f5s $^3F^o_2$	5s5d $^3D_1$	2.66E + 10	2.77E + 10	0.05
518.742	5s5d $^1D_2$	5s6p $^1P^o_1$	2.33E + 10	1.03E + 10	− 0.37
519.525	5s^2 $^1S_0$	5s5p $^1P^o_1$	4.08E + 10	3.88E + 10	0.19
521.162	4f5p $^3G_4$	5p5d $^3F^o_3$	1.76E + 10	1.63E + 10	− 0.15
532.394	5s5p $^3P^o_0$	5p^2 $^3P_1$	1.77E + 10	1.38E + 10	− 0.25
533.922	5s5p $^3P^o_2$	5p^2 $^3P_2$	4.15E + 10	3.42E + 10	0.15
539.881	4f5p $^3G_5$	5p5d $^3F^o_4$	2.48E + 10	2.52E + 10	0.07
540.570	4f5p $^3G_3$	5p5d $^3F^o_2$	1.38E + 10	1.39E + 10	− 0.19
545.280	5s5p $^3P^o_1$	5p^2 $^1D_2$	1.44E + 10	9.56E + 09	− 0.38
548.507	4f5s $^3F^o_3$	4f5p $^1G_4$	8.90E + 09	7.78E + 09	− 0.44
551.812	5s5p $^3P^o_1$	5p^2 $^3P_1$	1.12E + 10	8.89E + 09	− 0.41
552.313	4f5s $^3F^o_4$	4f5p $^1G_4$	6.70E + 09	5.80E + 09	− 0.56
554.078	4f5s $^3F^o_3$	4f5p $^1D_2$	4.20E + 09	1.96E + 09	− 1.04
564.314	5s5p $^1P^o_1$	5p^2 $^1S_0$	1.50E + 10	1.17E + 10	− 0.25
564.420	4f5s $^3F^o_2$	4f5p $^3D_1$	7.60E + 09	2.51E + 07	− 2.93
565.211	5s5d $^3D_2$	5p5d $^3D^o_3$	1.59E + 10	8.89E + 09	− 0.37
570.315	4f5s $^3F^o_2$	4f5p $^3D_3$	9.00E + 08	6.59E + 08	− 1.48
572.636	4f5s $^3F^o_3$	4f5p $^3D_3$	1.28E + 10	9.16E + 09	− 0.34
572.788	4f5s $^1F^o_3$	4f5p $^1G_4$	4.27E + 10	3.33E + 10	0.23
573.066	5s5d $^3D_3$	5p5d $^3D^o_3$	2.30E + 10	1.72E + 10	− 0.07
574.298	4f5s $^3F^o_2$	4f5p $^3D_2$	1.57E + 10	1.23E + 10	− 0.20
574.803	4f5s $^3F^o_4$	4f5p $^3G_5$	7.12E + 10	5.75E + 10	0.47
576.663	4f5s $^3F^o_3$	4f5p $^3D_2$	2.80E + 09	2.03E + 09	− 0.99
576.813	4f5s $^3F^o_4$	4f5p $^3D_3$	8.70E + 09	6.38E + 09	− 0.49
578.908	4f5s $^1F^o_3$	4f5p $^1D_2$	9.30E + 09	7.90E + 09	− 0.39
583.864	4f5s $^3F^o_3$	4f5p $^3F_4$	3.82E + 10	3.15E + 10	0.22
588.205	4f5s $^3F^o_4$	4f5p $^3F_4$	1.67E + 10	1.40E + 10	− 0.13
590.741	4f5s $^3F^o_2$	4f5p $^1F_3$	2.20E + 10	1.84E + 10	− 0.01
593.244	4f5s $^3F^o_3$	4f5p $^1F_3$	7.30E + 09	6.77E + 09	− 0.43
599.168	4f5s $^1F^o_3$	4f5p $^3D_3$	9.50E + 09	7.97E + 09	− 0.36
606.422	5s5d $^3D_3$	5p5d $^3F^o_4$	3.39E + 10	2.08E + 10	0.09
621.777	4f5s $^1F^o_3$	4f5p $^1F_3$	1.13E + 10	7.97E + 09	− 0.36
621.949	5s5d $^1D_2$	5p5d $^1F^o_3$	1.78E + 10	7.11E + 09	− 0.37
626.590	5s5p $^3P^o_1$	5p^2 $^3P_0$	1.06E + 10	8.70E + 09	− 0.32
627.593	5s5p $^3P^o_2$	5p^2 $^1D_2$	1.41E + 10	9.98E + 09	− 0.25
636.241	5s5p $^3P^o_2$	5p^2 $^3P_1$	1.28E + 10	1.05E + 10	− 0.22

Table 8 – *continued*

λ_{obs} (Å)[a]	Transition		gA (s^{-1})		log gf
	Lower level	Upper level	Previous[a]	This work[b]	This work[b]
654.123	5s5p $^1P^o_1$	5p^2 $^3P_2$	8.10E + 09	5.18E + 09	– 0.45
679.395	4f5s $^3F^o_3$	4f5p $^3G_4$	6.30E + 09	4.67E + 09	– 0.49
685.284	4f5s $^3F^o_4$	4f5p $^3G_4$	2.17E + 10	1.88E + 10	0.13
687.918	4f5s $^3F^o_2$	4f5p $^3F_2$	8.10E + 09	7.78E + 09	– 0.25
688.537	4f5s $^3F^o_3$	4f5p $^3F_3$	5.90E + 09	5.12E + 09	– 0.44
691.309	4f5s $^3F^o_3$	4f5p $^3F_2$	7.50E + 09	6.25E + 09	– 0.34
694.584	4f5s $^3F^o_4$	4f5p $^3F_3$	1.29E + 10	1.02E + 10	– 0.13
703.283	4f5s $^3F^o_2$	4f5p $^3G_3$	1.13E + 10	9.14E + 09	– 0.17
706.822	4f5s $^3F^o_3$	4f5p $^3G_3$	7.30E + 09	6.80E + 09	– 0.29
717.070	4f5s $^1F^o_3$	4f5p $^3G_4$	6.10E + 09	5.26E + 09	– 0.39
727.272	4f5s $^1F^o_3$	4f5p $^3F_3$	5.20E + 09	5.58E + 09	– 0.35
746.148	5s^2 $^1S_0$	5s5p $^3P^o_1$	9.00E + 08	5.30E + 08	– 1.32
747.702	4f5s $^1F^o_3$	4f5p $^3G_3$	5.70E + 09	4.69E + 09	– 0.40
800.455	5s5p $^1P^o_1$	5p^2 $^1D_2$	5.30E + 09	4.31E + 09	– 0.35

[a]Ryabtsev et al. (2002); [b]HFR + CPOL calculations.

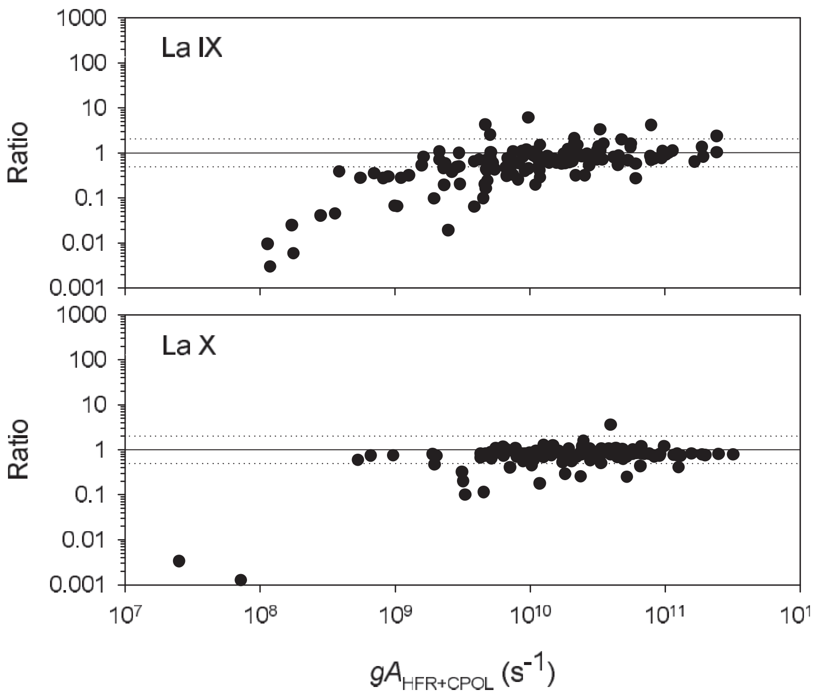

Figure 2. Comparison between HFR + CPOL transition probabilities (gA) and previously published values for experimentally observed lines in La IX and La X ions. For each ion, the ratio $gA_{HFR+CPOL}/gA_{Previous}$ is plotted against $gA_{HFR+CPOL}$. Previous data were taken from Churilov & Joshi (2001) for La IX and from Ryabtsev et al. (2002) for La X. The solid line corresponds to ratios equal to unity while the dotted lines correspond to deviations of a factor of 2.

Therefore the optical depth can be written as

$$\tau_l = \frac{\pi e^2}{m_e c}\left(\frac{n\lambda_l t}{g_0}\right) g_l f_l\, e^{-E_l/k_B T}. \quad (5)$$

In all the expressions given above, it is important to use the correct temperature. This can be estimated from the Saha equation:

$$\frac{n_j}{n_{j-1}} = \frac{U_j(T)U_e(T)}{U_{j-1}(T)n_e}\, e^{-\chi_{j-1}/k_B T}, \quad (6)$$

where n_j and n_{j-1} are the ionic densities in the j and $j-1$ charge stages, n_e is the electron density, χ_{j-1} is the ionization potential of the ion $j-1$, $U_j(T)$ and $U_{j-1}(T)$ are the partition functions for charge stages j and $j-1$, respectively, computed using all the energy levels, $E_i^{(j)}$ and $E_i^{(j-1)}$, and their statistical weights, $g_i^{(j)}$ and $g_i^{(j-1)}$, belonging to the corresponding ions:

$$U_j(T) = \sum_i g_i^{(j)}\, e^{-E_i^{(j)}/k_B T}, \quad (7)$$

$$U_{j-1}(T) = \sum_i g_i^{(j-1)}\, e^{-E_i^{(j-1)}/k_B T}. \quad (8)$$

The electronic partition function, U_e, is given by

$$U_e(T) = 2\left(\frac{m_e k_B T}{2\pi\hbar^2}\right)^{3/2}, \quad (9)$$

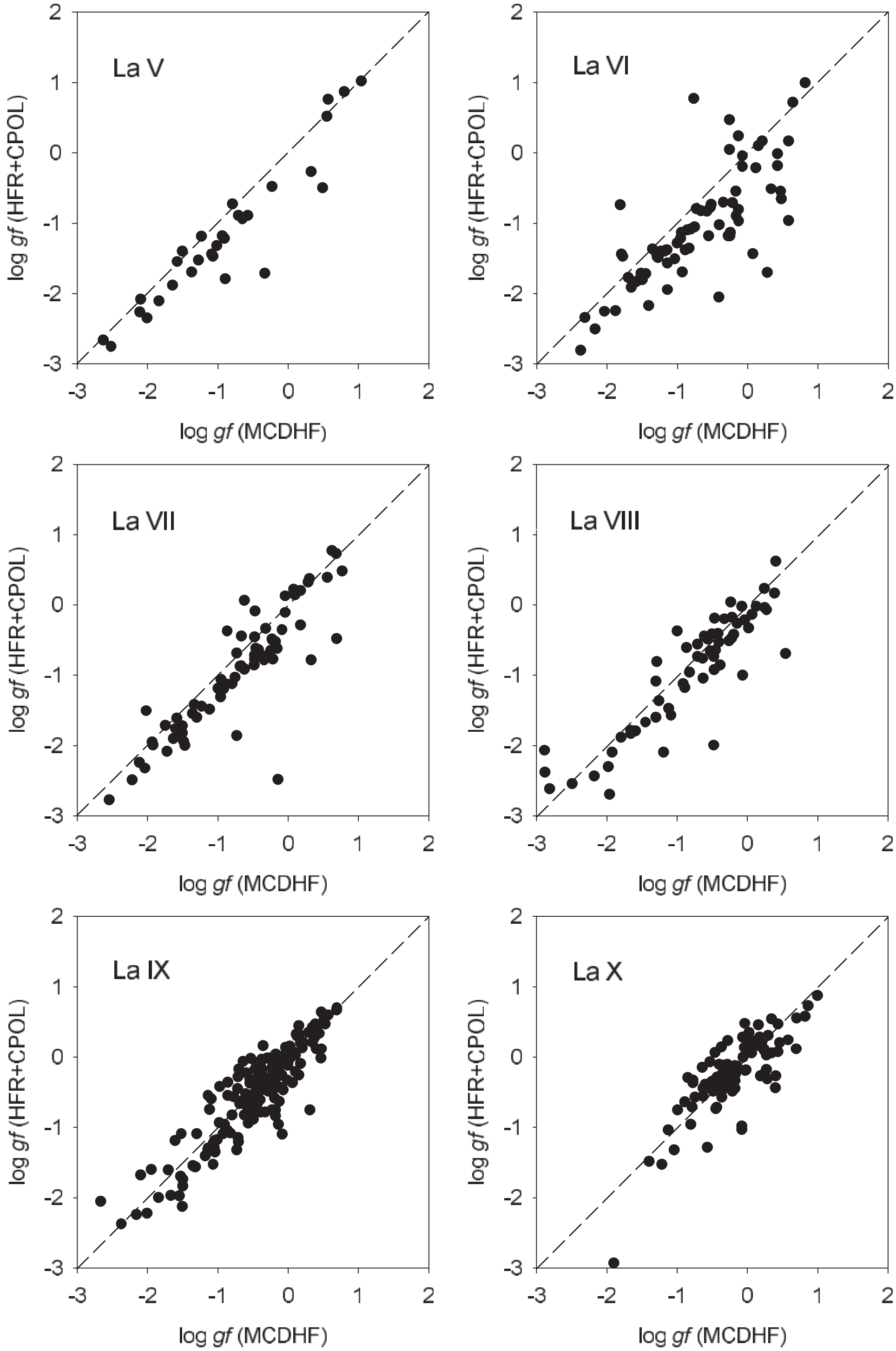

Figure 3. Comparison between oscillator strengths (log *gf*) computed in this work using the HFR + CPOL and MCDHF methods for experimentally observed lines in La V–X ions.

while the electron density, n_e, can be estimated, for an ionization degree *j*, using (see e.g. Banerjee et al. 2020)

$$n_e = \frac{\rho}{A m_p} j, \tag{10}$$

where *A* is the mass number and m_p is the proton mass.

Using the whole set of levels obtained in our HFR + CPOL calculations, the number of which is given in Table 9 and in Fig. 5, the partition functions of La V–X ions were computed for temperatures ranging from 1 to 100 000 K. These new partition functions, completed by those obtained for La I–IV ions by using the corresponding energy levels taken from the National Institute of Standards and Technology (NIST) data base (Kramida et al. 2019), were incorporated into the Saha equation to determine the relative number of lanthanum atoms in different ionization degrees, assuming a pure La gas. The ionization potentials taken from the NIST data

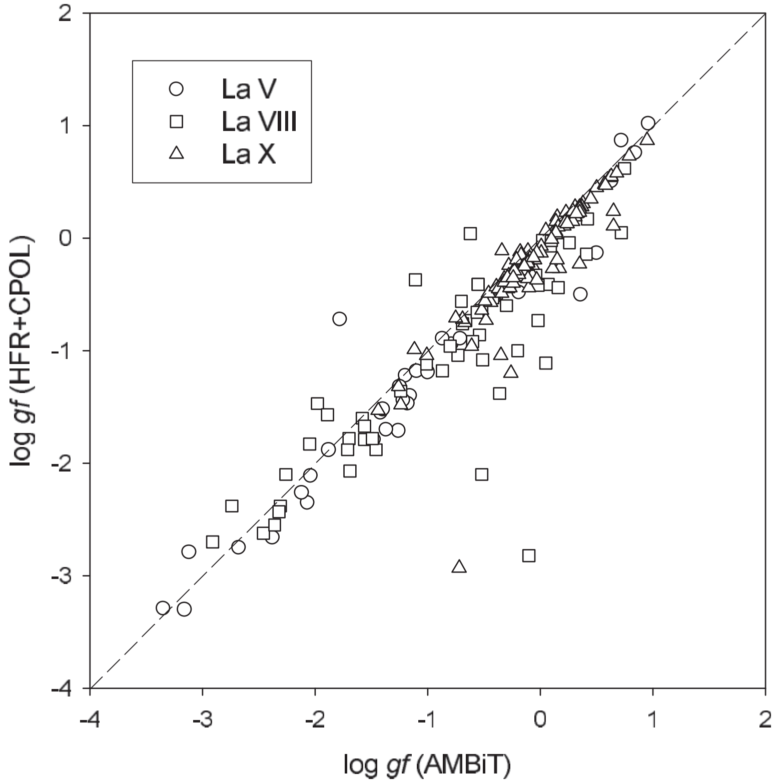

Figure 4. Comparison between oscillator strengths (log *gf*) computed in this work using the HFR + CPOL and AMBiT methods for experimentally observed lines in La V, La VIII, and La X ions.

Table 9. Number of levels and transitions obtained in HFR + CPOL calculations and used for opacity determination in La V–X ions. The ionization potentials and temperatures considered in opacity calculations are also given for each ion.

Ion	Levels[a]	Transitions[b]	IP (cm^{-1})[c]	T (K)[d]
La V	7816	308 724	497 000	25 000
La VI	7694	738 090	597 000	31 000
La VII	8292	818 233	710 000	38 000
La VIII	3971	749 088	847 000	45 000
La IX	1001	86 088	960 000	53 000
La X	380	17 024	1221 300	62 000

[a]Total number of levels considered in HFR + CPOL calculations.
[b]Total number of transitions considered in opacity calculations (see text).
[c]Ionization potential taken from NIST (Kramida et al. 2019).
[d]Temperature deduced in this work from the Saha equation and used in opacity calculations.

base (and reported in Table 3) were also included in the calculations while the mass density of the kilonova ejecta was assumed to range from $\rho = 10^{-13}$ to 10^{-10} g cm^{-3} when going from the first ionization degrees to higher ones, as suggested by Gaigalas et al. (2019) and Banerjee et al. (2020), respectively. The relative ionic lanthanum abundances thus obtained as a function of temperature are shown in Fig. 6, which led us to deduce that the temperatures corresponding to the maximum abundances could be estimated as 25 000 K for La V, 31 000 K for La VI, 38 000 K for La VII, 45 000 K for La VIII, 53 000 K for La IX, and 62 000 K for La X, as summarized in Table 9.

For each of the lanthanum ions, the bound–bound opacities were then computed with these temperatures, considering a density $\rho = 10^{-10}$ g cm^{-3} and a time after merger $t = 0.1$ d, as suggested by Banerjee et al. (2020) for the early phases of kilonovae in which La V–X are expected to be present. The wavelength width appearing in equation (2) was chosen to be $\Delta\lambda = 5$ Å, according to our previous works on opacity calculations in Ce II–IV (Carvajal Gallego et al. 2021) and Ce V–X (Carvajal Gallego et al. 2022) ions. Moreover, the HFR + CPOL radiative parameters obtained for all transitions with $\log gf > -5$ involving energy levels below the ionization potentials were included in the computations, this limit in log *gf* values having been shown to be realistic in previous studies (Fontes et al. 2020; Carvajal Gallego et al. 2022) to account for all transitions contributing significantly to opacities. For each lanthanum ion considered in this work, the final number of lines used for computing the opacities is given in Table 9. Note that this represents a total of nearly 3 million transitions spread over the six ions from La V to La X. The expansion opacities thus obtained are plotted versus wavelengths in Figs 7–12 for La V, La VI, La VII, La VIII, La IX, and La X, respectively, showing values ranging from 0.01 to about 10 cm^2 g^{-1}, depending on the ionization degree with a maximum value around 500 Å, similar to what we had obtained in the case of Ce V–X ions (Carvajal Gallego et al. 2022).

6 CONCLUSION

Large-scale calculations of atomic structures and radiative parameters were undertaken for lanthanum ions between La V and La X using three different computational approaches based on the HFR + CPOL, MCDHF, and AMBiT theoretical methods. Detailed comparisons between the results obtained with these three methods allowed us to deduce a reliable set of wavelengths, transition probabilities, and oscillator strengths for about 3 million lines spread over the six lanthanum ions of interest. These data were then used to compute the

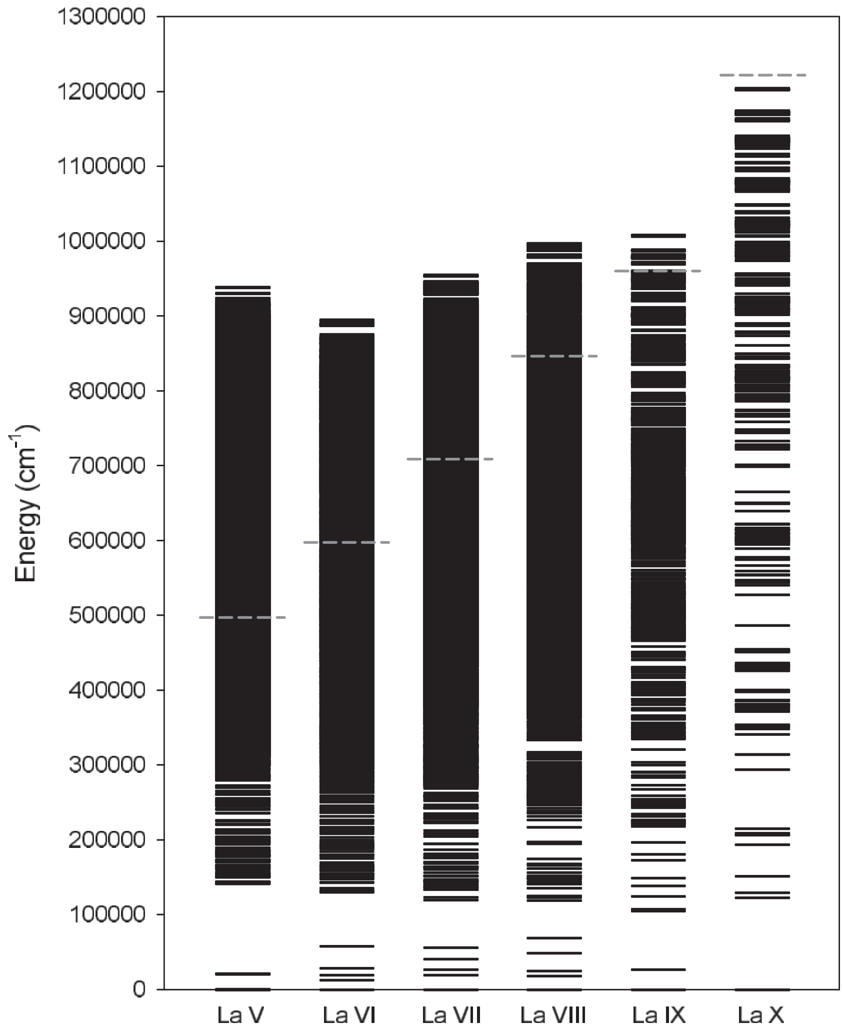

Figure 5. Full set of energy levels obtained in HFR + CPOL calculations. The dashed lines in grey correspond to the ionization potentials taken from the NIST data base (Kramida et al. 2019).

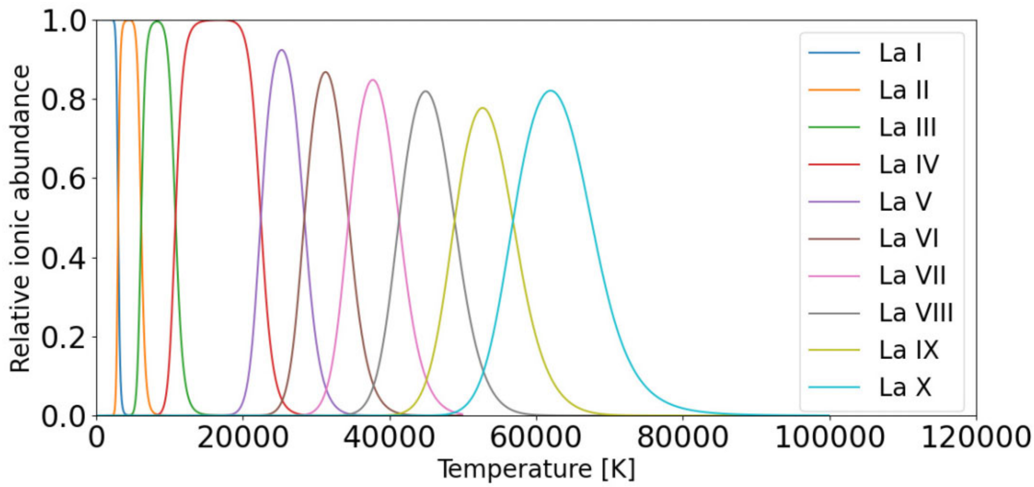

Figure 6. Relative ionic abundances for La I–X species as a function of temperature.

monochromatic opacities due to La V–X ions for the investigation of spectra emitted by early-phase kilonovae observed after neutron star mergers, i.e. for typical kilonova conditions such as $T > 20\,000$ K, $\rho = 10^{-10}$ g cm^{-3}, and $t = 0.1$ d.

The results presented in this paper are part of a systematic and detailed study concerning the radiative data and opacities characterizing the moderately charged lanthanide ions (V–X) recently initiated by our work on Ce V–X ions (Carvajal Gallego et al. 2022) and that

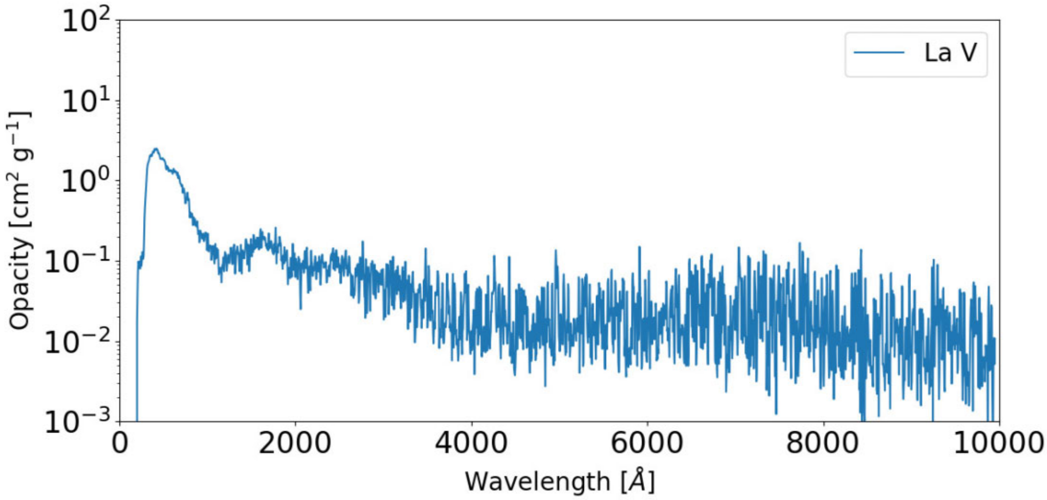

Figure 7. Expansion opacity for La V, calculated with $T = 25\,000$ K, $\rho = 10^{-10}$ g cm^{-3}, $t = 0.1$ d, and $\Delta\lambda = 5$ Å.

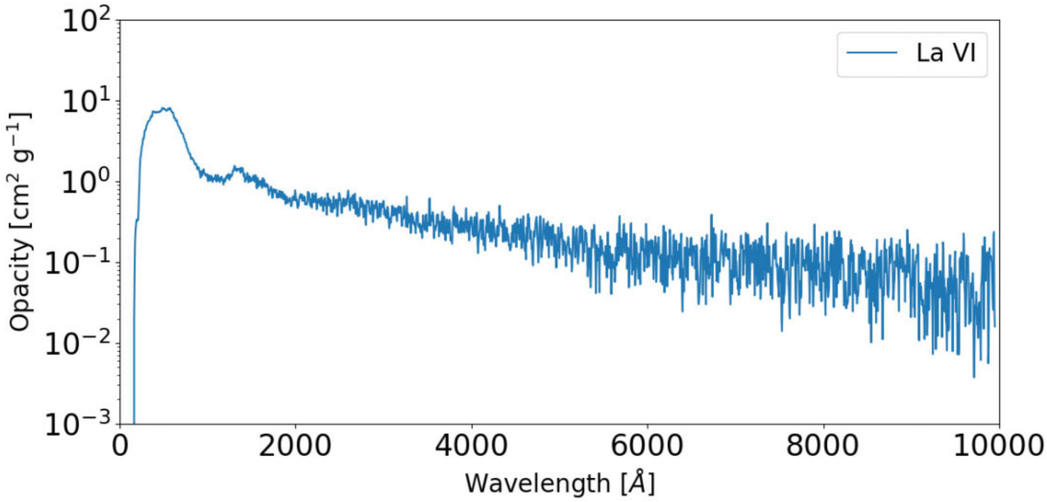

Figure 8. Expansion opacity for La VI, calculated with $T = 31\,000$ K, $\rho = 10^{-10}$ g cm^{-3}, $t = 0.1$ d, and $\Delta\lambda = 5$ Å.

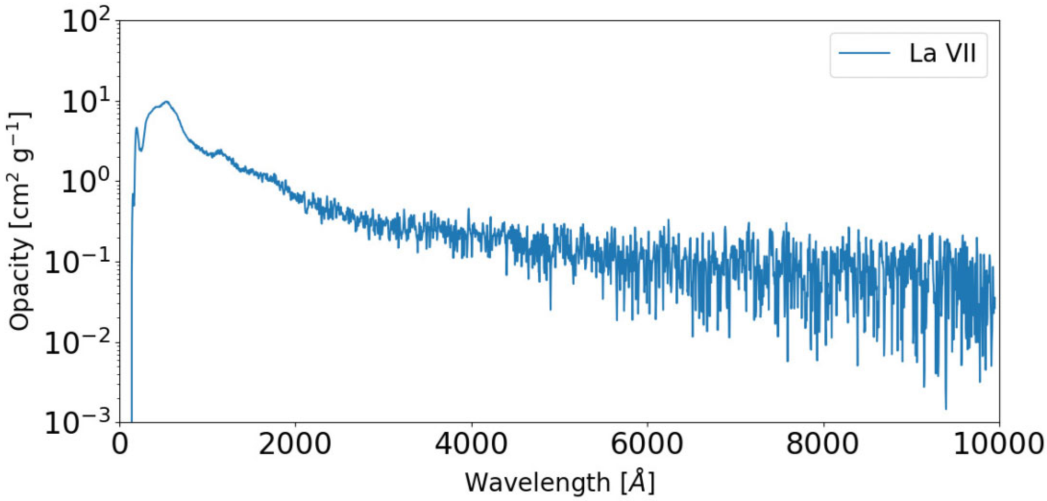

Figure 9. Expansion opacity for La VII, calculated with $T = 38\,000$ K, $\rho = 10^{-10}$ g cm^{-3}, $t = 0.1$ d, and $\Delta\lambda = 5$ Å.

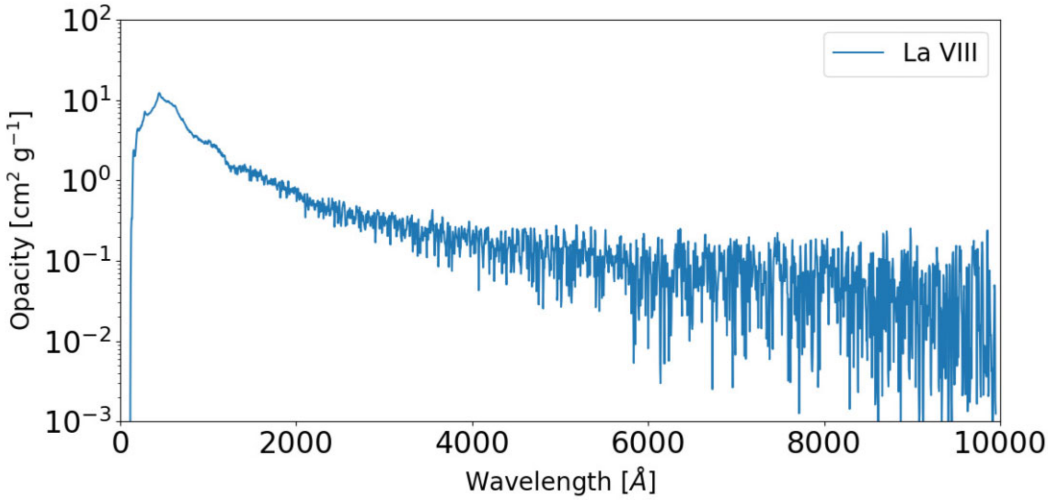

Figure 10. Expansion opacity for La VIII, calculated with $T = 45\,000$ K, $\rho = 10^{-10}$ g cm^{-3}, $t = 0.1$ d, and $\Delta\lambda = 5$ Å.

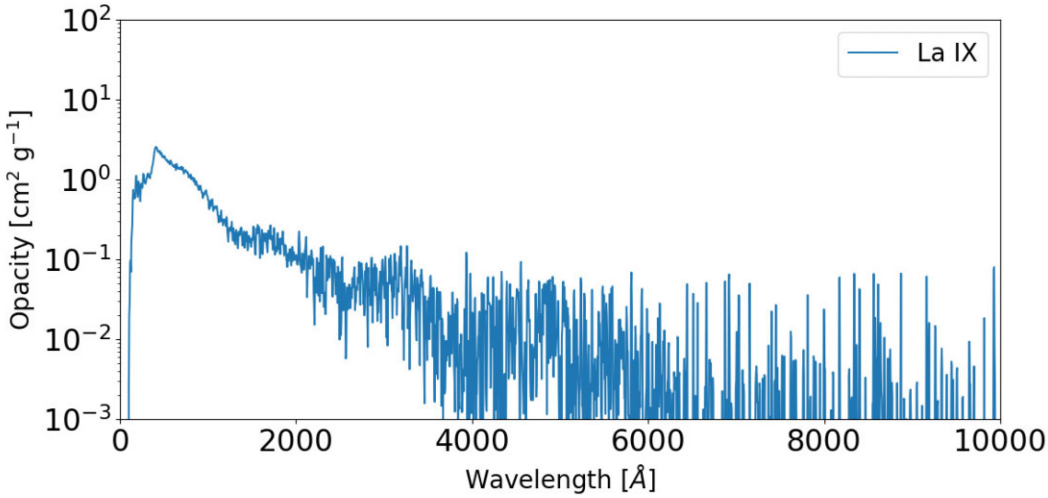

Figure 11. Expansion opacity for La IX, calculated with $T = 53\,000$ K, $\rho = 10^{-10}$ g cm^{-3}, $t = 0.1$ d, and $\Delta\lambda = 5$ Å.

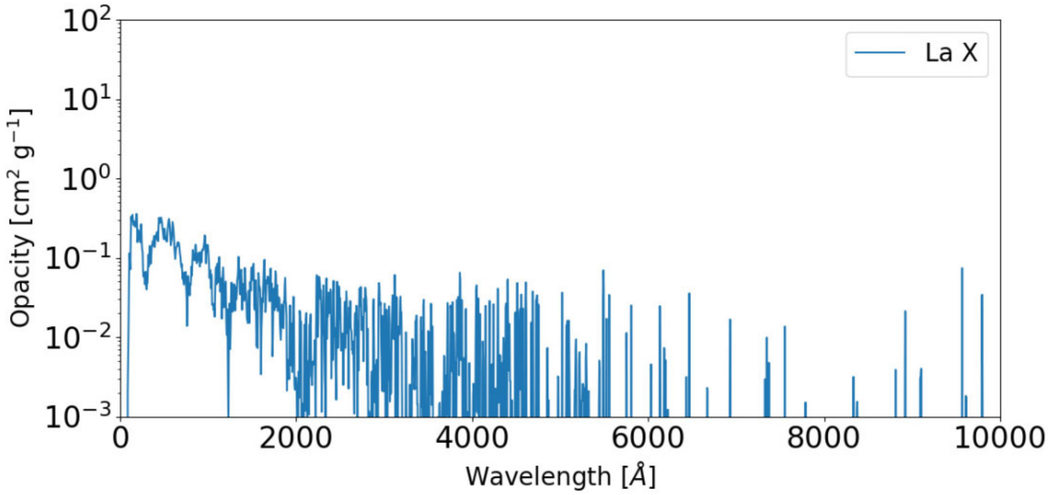

Figure 12. Expansion opacity for La X, calculated with $T = 62\,000$ K, $\rho = 10^{-10}$ g cm^{-3}, $t = 0.1$ d, and $\Delta\lambda = 5$ Å.

will continue with the analysis of other lanthanide ions in future papers.

ACKNOWLEDGEMENTS

HCG is holder of a FRIA fellowship while PP and PQ are, respectively, Research Associate and Research Director of the Belgian Fund for Scientific Research F.R.S. – FNRS. This project has received funding from the FWO and F.R.S. – FNRS under the Excellence of Science (EOS) programme (number O.0004.22). Computational resources have been provided by the Consortium des Équipements de Calcul Intensif (CECI), funded by the F.R.S. – FNRS under Grant No. 2.5020.11 and by the Walloon Region of Belgium.

DATA AVAILABILITY

The data underlying this paper will be shared on reasonable request to the corresponding author.

REFERENCES

Abbott B. P. et al., 2017a, Phys. Rev. Lett., 119, 161101
Abbott B. P. et al., 2017b, ApJ, 848, L13
Banerjee S., Tanaka M., Kawaguchi K., Kato D., Gaigalas G., 2020, ApJ, 901, 29
Berengut J. C., 2016, Phys. Rev. A, 94, 012502
Biémont E., Froese Fischer C., Godefroid M. R., Palmeri P., Quinet P., 2000, Phys. Rev. A, 62, 032512
Carvajal Gallego H., Palmeri P., Quinet P., 2021, MNRAS, 501, 1440
Carvajal Gallego H., Berengut J. C., Palmeri P., Quinet P., 2022, MNRAS, 509, 6138
Chou H.-S., Huang K.-N., 1992, Phys. Rev. A, 46, 3725
Churilov S. S., Joshi Y. N., 2001, Phys. Scr., 64, 34
Cowan R. D., 1981, The Theory of Atomic Structure and Spectra. California Univ. Press, Berkeley
Curtis L. J., Matulioniene R., Ellis D. G., Froese Fischer C., 2000, Phys. Rev. A, 62, 052513
Eastman R. G., Pinto P. A., 1993, ApJ, 412, 731
Epstein G. L., Reader J., 1976, J. Opt. Soc. Am., 66, 590
Fontes C. J., Fryer C. L., Hungerford A. L., Wollaeger R. T., Korobkin O., 2020, MNRAS, 493, 4143
Fraga S., Karwowski J., Saxena K. M. S., 1976, Handbook of Atomic Data. Elsevier, Amsterdam
Froese Fischer C., Godefroid M., Brage T., Jönsson P., Gaigalas G., 2016, J. Phys. B: At. Mol. Opt. Phys., 49, 182004
Froese Fischer C., Gaigalas G., Jönsson P., Bieroń J., 2019, Comput. Phys. Commun., 237, 184
Gaigalas G., Kato D., Rynkun P., Radžiūtė L., Tanaka M., 2019, ApJS, 240, 29
Gaigalas G., Rynkun P., Radžiūtė L., Kato D., Tanaka M., Jönsson P., 2020, ApJS, 248, 13
Gayasov R., Joshi Y. N., 1998, J. Opt. Soc. Am., 15, 2614
Gayasov R., Joshi Y. N., Tauheed A., 1997, J. Phys. B: At. Mol. Opt. Phys., 30, 873
Gayasov R., Joshi Y. N., Tauheed A., 1998, Phys. Scr., 57, 565
Gayasov R., Joshi Y. N., Ryabtsev A. N., 1999, Phys. Scr., 59, 419
Geddes A. J., Czapski D. A., Kahl E. V., Berengut J. C., 2018, Phys. Rev. A, 98, 042508
Grant I. P., 2007, Relativistic Quantum Theory of Atoms and Molecules: Theory and Computation. Springer, New York
Kahl E. V., Berengut J. C., 2019, Comput. Phys. Commun., 238, 232
Karp A. H., Lasher G., Chan K. L., Salpeter E. E., 1977, ApJ, 214, 161
Kasen D., Thomas R. C., Nugent P., 2006, ApJ, 651, 366
Kasen D., Metzger B., Barnes J., Quataert E., Ramirez-Ruiz E., 2017, Nature, 551, 80
Kaufman V., Sugar J., 1987, J. Opt. Soc. Am. B: Opt. Phys., 4, 1919
Kramida A., Ralchenko Yu., Reader J., NIST ASD Team, 2019, NIST Atomic Spectra Database (version 5.7.1.). National Institute of Standards and Technology, Gaithersburg, MD. Available online at https://physics.nist.gov/asd
Quinet P., 2017, Can. J. Phys., 95, 790
Quinet P., Palmeri P., 2020, Atoms, 8, 18
Quinet P., Palmeri P., Biémont E., McCurdy M. M., Rieger G., Pinnington E. H., Wickliffe M. E., Lawler J. E., 1999, MNRAS, 307, 934
Quinet P., Palmeri P., Biémont E., Li Z. S., Zhang Z. G., Svanberg S., 2002, J. Alloys Compounds, 344, 255
Radžiūtė L., Gaigalas G., Kato D., Rynkun P., Tanaka M., 2020, ApJS, 248, 17
Radžiūtė L., Gaigalas G., Kato D., Rynkun P., Tanaka M., 2021, ApJS, 257, 29
Reshetnikov N., Curtis L. J., Brown M. S., Irving R. E., 2008, Phys. Scr., 77, 015301
Ryabtsev A. N., Churilov S. S., Joshi Y. N., 2002, Phys. Scr., 65, 227
Sobolev V. V., 1960, Moving Envelopes of Stars. Harvard Univ. Press, Cambridge, MA
Tanaka M., Kato D., Gaigalas G., Kawaguchi K., 2020, MNRAS, 496, 1369
Tauheed A., Joshi Y. N., Marshall A., 2008, Phys. Scr., 77, 045301

This paper has been typeset from a TEX/LATEX file prepared by the author.